THE JOURNAL OF BIOLOGICAL CHEMISTRY VOL. 291, NO. 28, pp. 14483–14498, July 8, 2016

How Phosphorylation and ATPase Activity Regulate Anion Flux though the Cystic Fibrosis Transmembrane Conductance Regulator (CFTR)*

Received for publication, February 12, 2016, and in revised form, May 5, 2016 Published, JBC Papers in Press, May 12, 2016, DOI 10.1074/jbc.M116.721415

Matthias Zwick[1], **Cinzia Esposito, Manuel Hellstern, and Anna Seelig**[2]

From the Biophysical Chemistry, Biozentrum, University of Basel, Klingelbergstrasse 50/70, CH-4056 Basel, Switzerland

The cystic fibrosis transmembrane conductance regulator (CFTR, ABCC7), mutations of which cause cystic fibrosis, belongs to the ATP-binding cassette (ABC) transporter family and works as a channel for small anions, such as chloride and bicarbonate. Anion channel activity is known to depend on phosphorylation by cAMP-dependent protein kinase A (PKA) and CFTR-ATPase activity. Whereas anion channel activity has been extensively investigated, phosphorylation and CFTR-ATPase activity are still poorly understood. Here, we show that the two processes can be measured in a label-free and non-invasive manner in real time in live cells, stably transfected with CFTR. This study reveals three key findings. (i) The major contribution (≥90%) to the total CFTR-related ATP hydrolysis rate is due to phosphorylation by PKA and the minor contribution (≤10%) to CFTR-ATPase activity. (ii) The mutant CFTR-E1371S that is still conductive, but defective in ATP hydrolysis, is not phosphorylated, suggesting that phosphorylation requires a functional nucleotide binding domain and occurs in the post-hydrolysis transition state. (iii) CFTR-ATPase activity is inversely related to CFTR anion flux. The present data are consistent with a model in which CFTR is in a closed conformation with two ATPs bound. The open conformation is induced by ATP hydrolysis and corresponds to the post-hydrolysis transition state that is stabilized by phosphorylation and binding of chloride channel potentiators.

The cystic fibrosis transmembrane conductance regulator (CFTR,[3] ABCC7), with a molecular mass of ~140 kDa, is a channel for small anions such as chloride (or iodide) and bicarbonate (1). It belongs to the C-family of ATP-binding cassette (ABC) transporters (ABCC) and is composed of two homologous halves, each comprising a transmembrane (TMD) and a nucleotide binding domain (NBD). As other members of the ABCC family, CFTR lacks the catalytic glutamine in NBD1 and carries it only in NBD2 (Glu-1371) (2). In NBD1, glutamine is replaced by serine (Ser-573), which binds nucleotides tightly, but significantly reduces the rate of ATP hydrolysis (3). The two halves of the protein are linked by an intrinsically disordered (4) regulatory (R) domain, unique to CFTR. This leads to the overall domain organization TMD1-NBD1-R-TMD2-NBD2 (5). The R-domain is highly charged and contains numerous serine residues that can be phosphorylated by protein kinases, particularly by the cAMP-dependent protein kinase A (PKA) (6). A low resolution structure of CFTR, obtained by electron crystallography in the absence of nucleotides and phosphorylation (7), revealed strong similarity to the nucleotide-bound structure of the homodimeric bacterial ABC transporter Sav1866 (8).

The function of the CFTR anion channel has been investigated in great detail by different electrophysiological methods, including iodide efflux measurements with iodide-sensitive electrodes, Ussing chamber measurements, and most importantly patch clamp techniques (9). Although CFTR gating has long been known to depend on the hydrolysis of nucleoside triphosphate (generally ATP) (10, 11) and on phosphorylation of the R-domain (12), information on direct measurements of the two processes is sparse.

CFTR ATPase activity could so far be measured only with radioactively labeled nucleotides in inside-out membrane vesicles, as first demonstrated by Riordan and co-workers (13). The maximum rate of ATP hydrolysis by phosphorylated CFTR was determined as V_{max} = 53.8 nmol mg^{-1} min^{-1} (14), in good agreement with the catalytic rate constant or turnover number determined as k_{cat} ≈0.14 s^{-1} (15). However, CFTR shows significant (80–90%) functional attrition during reconstitution, and therefore the turnover number was later re-estimated as k_{cat} = 1–2 s^{-1} (16), which brings it into the time frame for channel gating (17). Further insight into the role of ATP hydrolysis was gained indirectly by investigating channel gating by means of electrophysiological methods in the presence of different nucleotides (3, 18).

CFTR phosphorylation by PKA was first measured with radioactively labeled ATP and subsequent immunoprecipitation of phosphorylated CFTR in inside-out vesicles (13, 19) and cells (6). Because separation of the two ATP-consuming processes, CFTR-ATPase activity and PKA activity, is difficult, the quantitative information of these approaches is limited. PKA-dependent CFTR activation was therefore analyzed mainly indirectly, again using electrophysiological methods (20, 21).

* This work was supported in part by the Swiss National Science Foundation Grant 3100A-107793. The authors declare that they have no conflicts of interest with the contents of this article.

[1] Recipient of a Werner Siemens-Foundation Ph.D. fellowship within the program "Opportunities for Excellence."

[2] To whom correspondence should be addressed: Biozentrum, University of Basel, Klingelbergstrasse 50/70, CH-4056 Basel, Switzerland. Tel.: 41-61-267-2206; Fax: 41-61-267-2189; E-mail: anna.seelig@unibas.ch.

[3] The abbreviations used are: CFTR, cystic fibrosis transmembrane conductance regulator; ABC transporter, ATP binding cassette transporter; CF, cystic fibrosis; cAMP, 3′5′-cyclic adenosine monophosphate; CPT, 8-(4-chlorophenylthio) cAMP (8-CPT-cAMP); fsk, forskolin; BHK, baby hamster kidney; ECAR, extracellular acidification rate; OCR, oxygen consumption rate; NBD, nucleotide binding domain; TMD, transmembrane binding domain; R, regulatory; MEMα, minimum essential medium α.

Mutation of serine residues (Ser-660, Ser-737, Ser-795, and Ser-813) revealed that none of the sites alone was essential. Simultaneous mutation of all four serine residues substantially reduced the PKA-stimulated current (22); yet mutation of as much as 10 serine residues did not fully eliminate the PKA-stimulated current (23). Notably, CFTR constructs lacking the R-domain were still conductive and even exhibited a somewhat higher affinity to nucleotides but shorter open times (24). The unphosphorylated R-domain was therefore assumed to inhibit CFTR channel opening by interfering with nucleotide binding and dimerization, rather than by stabilizing NBD dimer formation, as proposed earlier (25, 26).

Presently, the most accepted model for CFTR function assumes channel *opening* upon ATP binding at the interface between the two NBDs, with concomitant formation of an outward facing form (5, 27), and channel *closing* upon ATP hydrolysis at NBD2, with subsequent formation of an inward facing form (28, 29). The model corresponds to the alternating access mechanism (30), which has also been adapted to other ABC transporters (31). This model is supported by the outward facing structures of Sav1866 with two identical nucleotides bound (8, 32) and the inward facing (outward closed) structure of the nucleotide-free P-glycoprotein (33). Alternating access to CFTR was confirmed recently by testing the accessibility of cysteines in the transmembrane domain with cysteine-reactive probes. However, surprisingly, the "open state" of CFTR was facing inward, and the "closed state" of CFTR was facing outward (34). This finding raises new questions as to the role of the ATP hydrolysis cycle for CFTR anion channel function.

To circumvent problems with the susceptibility of CFTR to reconstitution, we measured the CFTR-related ATP hydrolysis rate in live Chinese hamster ovary (CHO) and baby hamster kidney (BHK) cells, stably transfected with human CFTR (CHO-CFTR and BHK-CFTR cells). As ATP is re-synthesized directly on demand, ATP hydrolysis can be monitored by measuring the extracellular acidification rate (ECAR), if cells work under glycolytic conditions (35–38), or the oxygen consumption rate (OCR), if cells work under conditions of oxidative phosphorylation (respiration) (39). In parallel, we measured iodide efflux under comparable experimental conditions. As phosphorylation agents, we used CPT-cAMP and forskolin. CPT-cAMP causes dissociation of the regulatory and catalytic subunits of PKA, which leads to R-domain phosphorylation by the catalytic subunit, whereas forskolin acts indirectly by stimulating cAMP synthesis through adenylate cyclase. In the presence of CPT-cAMP, the energy required to drive CFTR activity (total CFTR-related ATPase activity) can thus be subdivided into the energy consumed to drive PKA and CFTR-ATPase activity, respectively. In the presence of forskolin, adenylate cyclase activity may also contribute.

The following questions were asked. (i) How much ATP is consumed by the individual processes contributing to the total CFTR-related ATP consumption rate, PKA, CFTR-ATPase, and adenylate cyclase activity, respectively? (ii) At which step of the CFTR-ATPase activity cycle does phosphorylation of the R-domain occur? (iii) How are phosphorylation of the R-domain by PKA and CFTR-ATPase activity related to anion efflux? The answers to these questions allowed unraveling the complex interplay between CFTR phosphorylation, CFTR-ATPase activity, and anion flux. A new model for the CFTR-ATPase activity cycle is proposed.

Experimental Procedures

Compounds—Capsaicin, CFTRinh-172, genistein, glibenclamide, glipizide, 8-(4-Chlorophenylthio)-AMP (CPT-cAMP), forskolin, methotrexate, and H-89 were obtained from Sigma. Myristoylated PKI(14–22), minimum essential medium (MEMα), DMEM, Dulbecco's PBS, fetal bovine serum (FBS), and other chemicals needed for cell culture were purchased from LuBioScience (Luzerne, Switzerland). CPT-cAMP, PKI(14–22), and H-89 stock solutions were prepared in water and forskolin solution in DMSO. The DMSO concentrations in cells always remained low, C_{DMSO} <0.5% (v/v), and had no influence on cellular metabolism in agreement with previous measurements (38). Methotrexate for cell culture was prepared as 100 mg/ml stock in sterile 1 N NaOH.

Cell Lines—CHO and BHK cell lines stably transfected with the human *CFTR* (CHO-CFTR, BHK-CFTR) or *CFTR-E1371S* (BHK-E1371S) gene were the generous gifts from Dr. J. R. Riordan (University of North Carolina) and Dr. Jürgen Reinhardt (Novartis, Switzerland).

Growth and Flow Media—For cell growth, MEMα without ribonucleosides and deoxyribonucleosides, containing 10% heat-inactivated FBS, was used.

For flow medium preparation, commercially available dry powder MEMα (for CHO cells) or DMEM (for BHK cells) was used. Both flow media were without FBS and without sodium bicarbonate to maintain a very low buffer capacity. Sodium chloride was used as a substitute to preserve osmotic balance. The pH was adjusted to 7.4 at 37 °C.

Cell Culture—Non-transfected CHO cells were grown in MEMα at 37 °C and 5% CO_2. Stably transfected cell lines were cultured in the same medium supplemented with 50 μM methotrexate. Cells were split 1:15 and passaged every 2–3 days. BHK cell lines expressing *CFTR* variants were grown in DMEM/F-12, 1:1, supplemented with 10% FBS and 500 μM methotrexate under the same conditions as CHO cells.

ECAR and OCR Measured with a Bionas—The Bionas Discovery® 2500 cell-analyzing system (39) consists of six parallel measuring chambers. Cells were directly seeded on Bionas SC1000 metabolic chips with oxygen, pH, and impedance sensors to reach a final number of $n = 3{\cdot}10^5$ cells per chip, which all contributed to the ECAR. The pH sensors measure the voltage change as a function of time that is linearly related to a pH change as a function of time. Oxygen sensors measure the current change as a function of time that is linearly related to oxygen concentration in solution as a function of time (for calibration, see below).

Cells were incubated for 4 h with growth medium. To start a stimulation cycle, cells were switched to flow medium with a flow rate, $r = 110$ μl/min in each measuring chamber, until a stable basal metabolic rate was reached (about 2 h). Cells were then exposed to medium containing phosphorylation agents, until a steady state was reached. After each stimulation cycle, cells were flushed again with pure medium until basal activity was reached, to ensure that stimulations were fully reversible. Arrival of the titrant

in the measurement chamber was monitored from changes in impedance values and was moreover calculated taking into account the dimensions of the tubing system. Pump cycles consisted of a 2-min go and a 2-min stop, yielding a time resolution of 4 min. Acidification was measured in the stop phase.

ECAR Measured with the Cytosensor—The Cytosensor® microphysiometer (Molecular Devices) (35, 40) consists of eight light-addressable potentiometric sensors. It offers a second tubing system that was filled with flow medium containing the titrant (*e.g.* CPT-cAMP or forskolin) and allows applying agents with little delay, as a valve close to the measurement chamber can be switched between the two channels. Because of the shorter tubing system, compound adsorption to the walls of the tubes is comparatively low.

Cells were grown as a layer on 3.0-μm polycarbonate membranes (inner diameter, 12 mm, Corning) on the bottom of a flow chamber in diffusive contact with the sensors. The sensors again measure the voltage change as a function of time. Cells were seeded to reach a final number of $N_C = 5{\cdot}10^5$ cells per membrane, corresponding to 80–90% confluency; however, because of the flow cell geometry, only ~33% of the cells contribute to the ECAR signal detected by the sensors ($N_C = 1.65{\cdot}10^5$ cells). Cells were incubated either for 4 h or overnight with growth medium, which was then switched to flow medium with a flow rate, $r = 100$ μl/min. Extracellular acidification rates were calculated using Molecular Devices Cytosoft®, and the slope between 5 s after stopping and 2 s before restarting the pump was evaluated to avoid artifacts caused by pump switching (for pump cycle see Fig. 1 in Ref. 41). The Cytosensor showed a time resolution of 2 min. To quantify the observed ECAR changes, four measurement points at the end of each drug exposure period were averaged and normalized to the average of the last four points of the basal ECAR before substance application, taken as 100%.

Quantification of Acid Export—The measured voltage change per time $ECAR_V$ ($\mu V\ s^{-1}$) was transformed to the effective ECAR (protons released $cell^{-1}\ s^{-1}$) based on a calibration (cal) showing that 61.0 ± 1.1 mV corresponded to 1 pH unit in the Cytosensor (37) and 48.0 ± 2.5 mV to 1 pH unit in the Bionas as shown in Equation 1,

$$ECAR = ECAR_V \cdot \beta \cdot V \cdot N_A/(cal \cdot N_C) \qquad \text{(Eq. 1)}$$

The buffer capacity of the flow medium was determined as $\beta =$ 0.596 mM, taking into account phosphate salts (0.91 mM) and the amino acids glutamine (2 mM), histidine (0.2 mM), and cysteine (0.57 mM) (42). The volumina of the flow chambers were $V = 2.8$ μl for the Cytosensor, and $V = 5.65$ μl for the Bionas. N_A is the Avogadro number, and N_C is the number of cells contributing to the ECAR ($N_C = 1.65{\cdot}10^5$ in Cytosensor and $N_C = 3{\cdot}10^5$ in Bionas).

Lactate Quantification—Experiments in the Cytosensor were carried out as described above, but the flow medium was replaced by phosphate buffer (0.3 mM $CaCl_2$, 0.6 mM $MgCl_2$, 0.5 mM KH_2PO_4, 3 mM KCl, 0.5 mM Na_2HPO_4, 130 mM NaCl, 10 mM glucose). The buffer was collected after leaving the measurement chamber. All cells contributed to lactate efflux. The samples were lyophilized and dissolved again in 3 ml of buffer (1 M glycine, 0.6 M hydrazine, 5.6 mM EDTA) at pH 9.5. Lactate dehydrogenase (5000 units/ml) and NAD (2.5 mM) were added to the buffer, and the absorbance increase at 340 nm was monitored. Lactate concentrations were calculated from the stable absorption at 340 nm reached at the end of the reaction (37).

Quantification of Oxygen Consumption—Assuming that the measured current $I(k)$ changes linearly with the oxygen concentration in solution, the oxygen consumption per time $\Delta n/\Delta t$ (mol s^{-1}) was determined as shown in Equation 2,

$$\frac{\Delta n}{\Delta t} = V_{r,\,chip} \cdot C_{O_{2S}} \left(\frac{\Delta I(k)}{\Delta t \cdot I_{bas}(k)} \right) \qquad \text{(Eq. 2)}$$

where $I(k)$ corresponds to ~1 nA and was set to 100% in each go phase to correct for the potential drift; $C_{O2,\,S}$ is the concentration of oxygen in aqueous solution at 37 °C ($C_{O2,\,S} = 0.214$ mM); $\Delta I(k)$ is the measured change in current (*e.g.* $\Delta I(k) = 1.5$ pA) reflecting the change in oxygen consumption, and $V_{r,\,chip}$ is the volume of the flow chamber ($V_{r,\,chip} = 5.65$ μl).

ATP Hydrolysis Rates—ATP hydrolysis rates were calculated taking into account that glycolysis yields two molecules of lactic acid per molecule of glucose consumed and produces two molecules of ATP. Respiration yields ~36 molecules of ATP per molecule of glucose, whereas six molecules of dioxygen are consumed (35). One molecule of dioxygen consumed thus corresponds to six molecules of ATP produced (42).

Iodide Efflux Measurements—Iodide efflux measurements were carried out according to Chen *et al.* (43) with small modifications. CHO cells were grown to 90% confluence in 60-mm culture dishes and were washed three times with 2.5 ml of loading buffer, pH 7.4, in which chloride was replaced by iodide (136 mM NaI, 3 mM KNO_3, 2 mM $Ca(NO_3)_2$, 11 mM glucose, 20 mM HEPES/NaOH). After incubation for 3 h in the dark at 37 °C, cells were washed carefully 30 times with 2.5 ml of efflux buffer, pH 7.4, in which chloride was replaced by nitrate (136 mM $NaNO_3$, 3 mM KNO_3, 2 mM $Ca(NO_3)_2$, 11 mM glucose, 20 mM HEPES/NaOH) to remove excess iodide. For iodide efflux measurements, efflux buffer was exchanged in 1-min intervals. After 5 min, efflux buffer was replaced by stimulation buffer (*i.e.* efflux buffer containing CPT-cAMP or forskolin). Samples were collected and stored in the dark at room temperature. An iodide-selective electrode (Mettler Toledo, perfectIon® combination I^-) was used to measure voltages of the samples. Iodide concentrations were calculated using a calibration curve obtained with efflux buffer containing various concentrations of NaI. All experiments were carried out at 37 °C.

Models—PKA activation by CPT-cAMP was fitted with Equation 3 as proposed previously for PKA in solution (44),

$$ECAR = 100 + (ECAR_{max} - 100) \left(\frac{C(CPT)}{K_{d,\,app} + C(CPT)} \right)^4 \qquad \text{(Eq. 3)}$$

The term in brackets reflects the activation of PKA by binding four cAMP molecules to the regulatory subunit and subsequent dissociation of regulatory and catalytic subunits.

The CFTR-ATPase activity *versus* modulator concentration curves were fitted with Equation 4, which is based on a

two-site binding model previously proposed for P-glycoprotein (38, 45).

$$V = \frac{K_1K_2V_0 + K_2V_1C + V_2C^2}{K_1K_2 + K_2C + C^2} \quad \text{(Eq. 4)}$$

Here V is the velocity reflecting the change in ATPase activity or ECAR; K_1 is the concentration of half-maximum activation; K_2 is the concentration of half-maximum inhibition; V_0 is the normalized basal activity; V_1 is the maximum activity; V_2 is the minimum activity, and C the allocrite concentration in aqueous solution. Experiments were performed under steady state conditions.

Results

Glycolysis and Oxidative Phosphorylation—Cultured cells generally work under glycolytic conditions in the presence of glucose as a carbon source (35). However, they possess the ability to shift dynamically between glycolysis and oxidative phosphorylation (or respiration) (46). To test which of the two metabolic pathways predominates under the present conditions, we measured the ECAR and the OCR of CHO-K1 and CHO-CFTR cells in flow medium without and with the phosphorylation agents CPT-cAMP and forskolin. Seven stimulation cycles were measured in sequence with increasing concentrations of CPT-cAMP (Fig. 1, *A* and *B*) and forskolin (Fig. 1, *C* and *D*), using a Bionas Discovery 2500. CPT-cAMP barely influenced the ECAR of CHO-K1 control cells (Fig. 1*A*). Conversely, it strongly stimulated the ECAR of CFTR-transfected cells (Fig. 1*B*). ECAR maxima were reached at incubation times, $t \sim 20$ min. The OCR increased only at the highest CPT-cAMP concentrations ($C_{CPT} > 100\ \mu$M) and was delayed by about 24 min relative to the ECAR.

The effect of forskolin was again small in CHO-K1 cells (Fig. 1*C*) and significantly more pronounced in CHO-CFTR cells (Fig. 1*D*). At higher forskolin concentrations (5th stimulation), the ECAR started to decrease and the OCR to increase in CHO-K1 and CHO-CFTR cells, indicating a decrease in glycolysis and an increase in respiration in both cell types. At even higher concentrations (6th stimulation), respiration became predominant. Washout (*i.e.* flushing cells with pure medium) after stimulation with high forskolin concentrations led to dilution of the compound and, as a consequence, to an ECAR rebounce. Whereas basal OCR was reached relatively rapidly (within a few minutes), the basal ECAR was reached only slowly (within more than an hour). Analogous washout effects, although with smaller amplitudes, were observed in CHO-K1 cells (see 6th stimulation).

In conclusion, CHO-K1 and CHO-CFTR cells worked under glycolytic conditions (yielding two molecules of ATP per molecule of glucose) in pure medium, as well as in the presence of CPT-cAMP up to the highest concentrations at incubation times, $t < 24$ min. In the presence of low forskolin concentrations ($C_{fsk} = 0.1–1\ \mu$M), the situation was identical. However, at higher concentrations, forskolin reduced cellular glucose uptake (47–49) and as a consequence cells shifted from glycolysis to the more efficient respiration (yielding ~36 molecules of ATP/molecule of glucose) (Table 1, end).

ECAR in CHO-K1 and CHO-CFTR Cells Measured as a Function of CPT-cAMP and Forskolin Concentration—For quantitative data evaluation, we repeated titrations of CHO-K1 and CHO-CFTR cells with CPT-cAMP and forskolin using a Cytosensor (that measures only the ECAR), because it shows less adsorption of hydrophobic compounds to the tubing system and has a higher time resolution. The ECAR of CHO-K1 and CHO-CFTR cells is shown as a function of the CPT-cAMP (Fig. 2*A*) and forskolin (Fig. 3*A*) concentration, respectively. As in Fig. 1*A*, CHO-K1 cells showed only a low response with a maximum of 142 ± 9% at high CPT-cAMP concentrations ($C_{CPT} \geq 200\ \mu$M), whereas CHO-CFTR cells again showed a significant ECAR increase with a maximum ECAR of 195 ± 20% at $C_{CPT} = 400\ \mu$M.

In the case of forskolin, the ECAR of CHO-K1 cells remained at the basal level at low concentrations, increased only slightly (maximum 125 ± 18%) at higher concentrations up to $C_{fsk} = 10\ \mu$M, and then decreased below basal values, reaching only ~50% of initial basal value at $C_{fsk} = 100\ \mu$M. The ECAR of CHO-CFTR cells increased already at low concentrations ($C_{fsk} < 1\ \mu$M) and reached a maximum of 195 ± 20% at the concentration $C_{fsk} = 1\ \mu$M. At higher concentrations, the ECAR started to decrease as for CHO-K1 cells and reached only 30% of the initial basal value at the concentration $C_{fsk} = 100\ \mu$M. As seen in Fig. 1, *C* and *D,* the decrease in ECAR is compensated by an increase in OCR and can be attributed to a shift from glycolysis to respiration in CHO-K1 and CHO-CFTR cells.

ECAR Corresponds to Lactate Efflux and Reflects the Rate of ATP Hydrolysis—To test whether the ECAR induced upon stimulation with CPT-cAMP corresponds to lactate export, we superfused CHO-CFTR cells with 50 μM CPT-cAMP for 2 h and collected the medium after it had passed the measurement chambers. Lactate was then quantified as described under "Experimental Procedures" (37). Basal acidification rates were determined as $\nu_L \approx 4{\cdot}10^6$ lactic acid molecules extruded cell^{-1} s^{-1}, which corresponds to $\nu_{ATP} \approx 4{\cdot}10^6$ ATP molecules cell^{-1} s^{-1} hydrolyzed via glycolysis. Upon stimulation with CPT-cAMP ($C_{CPT} = 50\ \mu$M), lactate efflux increased to 180 ± 10% relative to basal values (100%) corresponding to $\nu_L = 7.2{\cdot}10^6$ lactic acid molecules extruded cell^{-1} s^{-1}. The values obtained by lactate determination are in close agreement with the values obtained by ECAR measurements (see below) and confirm that cells worked under glycolytic conditions.

ATP Hydrolysis Rate Derived from ECAR and OCR—The basal ECAR of CHO-K1 and CHO-CFTR cells, respectively, was determined as $\nu_{bas,\,H} = 4.22{\cdot}10^6 \pm 0.44$ protons cell^{-1} s^{-1} (~0.42 amol cell^{-1} min^{-1}) if measured with the Bionas and as $\nu_{bas,\,H} = 4.94{\cdot}10^6 \pm 0.46$ protons cell^{-1} s^{-1} ($\nu_{bas,\,H} \approx 0.49$ fmol cell^{-1} min^{-1}) if measured with the Cytosensor for both cell lines (see Equation 1). As shown above, the protons measured corresponded to lactic acid molecules extruded.

The basal oxygen consumption rates of CHO-CFTR and CHO-K1 were determined as $\nu_{bas,\,ox} = 0.63$ fmol cell^{-1} min^{-1} for both cell lines (see Equation 2). This value is within the range of published basal oxygen consumption rates (ν_{oxygen} = 0.1–10 fmol cell^{-1} min^{-1}) (50). The basal ECAR and OCR values (100%) were used for further quantification.

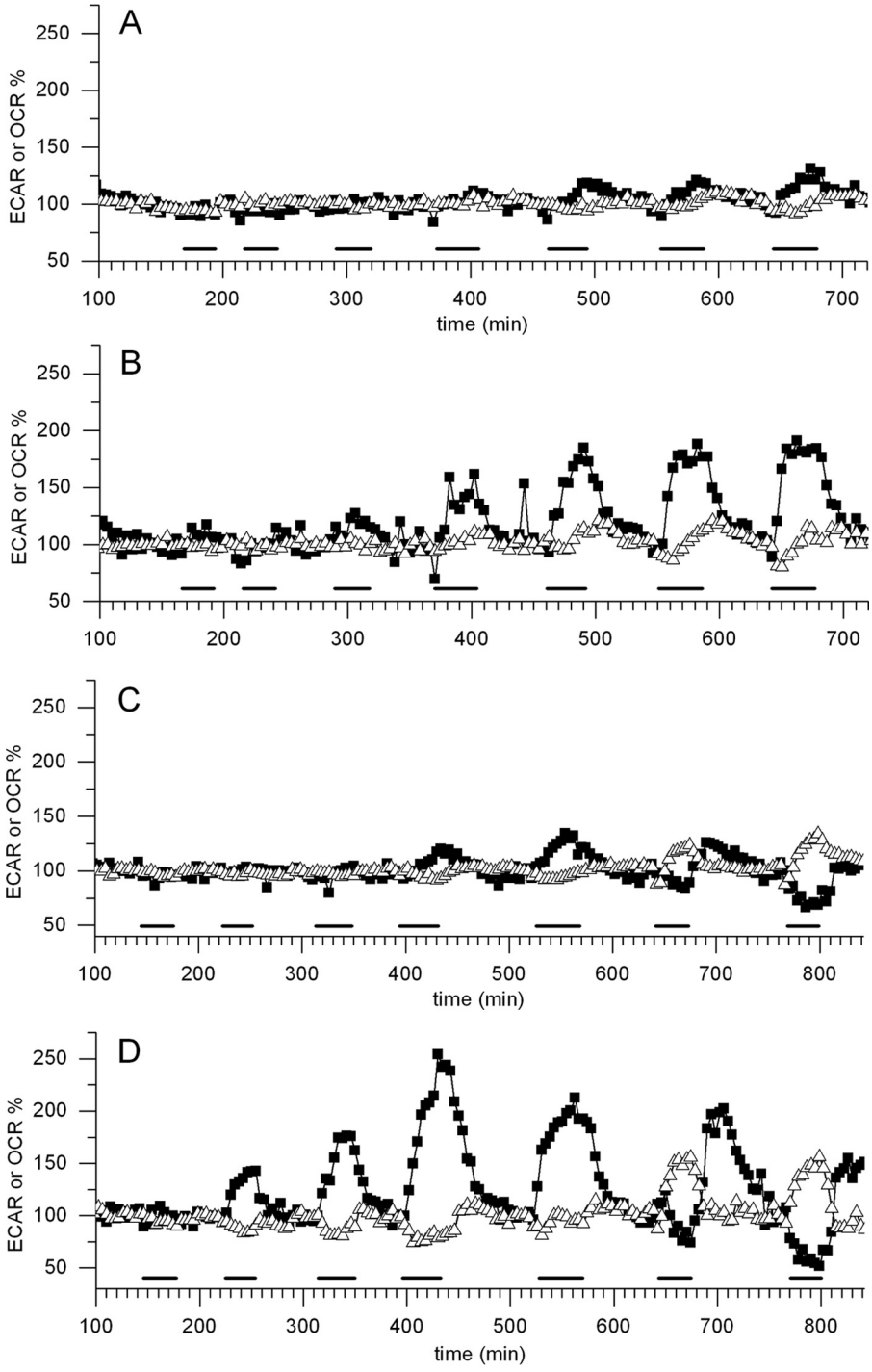

FIGURE 1. ***A–D,*** **ECAR and OCR of CHO-K1 and CHO-CFTR cells upon titration with CPT-cAMP and forskolin measured with a Bionas Discovery® 2500.** ECAR (■) and OCR (△) of CHO-K1 (*A*) and CHO-CFTR cells (*B*) at increasing concentrations of CPT-cAMP (C_{CPT} = 1, 5, 10, 50, 100, 200, and 320 μM) are shown. ECAR (■) and OCR (△) of CHO-K1 (*C*) and CHO-CFTR cells (*D*) at increasing concentrations of forskolin ($C_{fsk,\ applied}$ = 0.1, 1, 2, 5, 10, 50, and 100 μM) are shown. Measurements were performed at 37 °C. Rates were measured for 2 min, followed by 2 min of flushing with flow medium; a measurement point was thus generated every 4 min. *Horizontal lines* indicate the presence of phosphorylation agents in flow medium. Cells were stimulated with phosphorylation agents during 24 min at low concentrations and 32 min at higher concentrations. The concentrations given correspond to the concentrations applied; as the hydrophobic forskolin adsorbed to the tubing system, the concentrations reaching the measuring chambers were somewhat lower. Washout with pure flow medium after application of high forskolin concentrations induced an ECAR re-bounce due to forskolin dilution.

The ATP hydrolysis rate as a function of the CPT-cAMP concentration as derived from ECAR values (Fig. 2*A*) is shown in Fig. 2*B*. The ATP hydrolysis rate at t = 40 min was calculated by taking into account the OCR measured with the Bionas (last stimulation points in Fig. 1*B*). After correction for OCR, the ATP hydrolysis rates measured at the two different time points (t = 20 and 40 min) were identical, suggesting that phosphorylation reached a steady state at 20 min.

The ATP hydrolysis rate as a function of forskolin concentration (Fig. 3*B*) was estimated, combining ECAR (Fig. 3*A*) and

TABLE 1
Present and previous parameters related to PKA, CFTR-ATPase, and CFTR channel activity

Agent	Function	Parameter	Ref.
CPT	PKA activity	cAMP dissociation constant in CHO-CFTR cells, $K_{d,app} \approx 8.5\ \mu M$	Present
CPT	PKA activity	cAMP dissociation constant in BHK-CFTR cells, $K_{d,app} \approx 3.7\ \mu M$	Present
CPT	PKA activity	cAMP dissociation constant in aqueous solution, $K_{d,app} \approx 2.9\ \mu M$	56
CPT	PKA activity	Apparent half-max. phosphorylation (t = 20 min), $K_{0.5} \approx 40\ \mu M$	Present
CPT	PKA activity	Apparent half-max. phosphorylation (t = 8 min), $K_{0.5} \approx 40\ \mu M$	Present
CPT	PKA activity	Apparent half-max. phosphorylation (t = 6 min), $K_{0.5} \approx 63\ \mu M$	Present
CPT	PKA activity	Apparent half-max. phosphorylation (t = 4 min), $K_{0.5} \approx 83\ \mu M$	Present
CPT	PKA activity	Apparent half-maximal channel activation, $K_{0.5} \approx 80\ \mu M$	9
CPT	CFTR-ATPase	Partially phosphorylated: approximate catalytic rate constant, $k_{cat} = 14\ s^{-1}$	Present
CPT	CFTR-ATPase	Fully phosphorylated: app. catalytic rate constant, $k_{cat} = 1\text{-}2\ s^{-1}$	16
CPT	CFTR I^- efflux	ATP-independent increase at $C_{CPT} > 400\ \mu M$	Present
Fsk	CFTR I^- efflux	ATP-independent increase at $C_{fsk} > 15\ \mu M$	Present
Fsk	Metabolism	Cells shift from glycolysis to respiration at $C_{fsk} > 10\ \mu M$[a]	Present
Fsk	Metabolism	Metabolic effects $C_{fsk} > 20\ \mu M$	9

[a] Effect starts gradually and becomes dominant at $C_{fsk} > 10\ \mu M$.

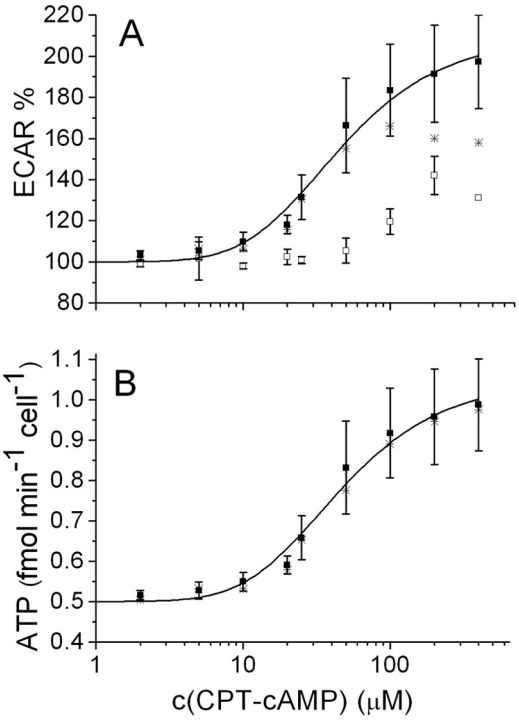

FIGURE 2. ***A* and *B*. ECAR of CHO-K1 and CHO-CFTR cells as a function of CPT-cAMP concentration.** ECAR of CHO-K1 (□) and CHO-CFTR (■) cells measured with a Molecular Dynamics Cytosensor at 37 °C for 30 s every 2 min is shown. *A*, either the average of the last four points of the measurements during perfusion with CPT-cAMP for ~20 min (ECAR maximum) (■) or 40 min (*) was normalized to the basal value before stimulation and was plotted against CPT-cAMP concentration. Extended superfusion (40 min) at high forskolin concentrations was used to monitor a potential ECAR decrease, reflecting the transition from glycolysis to respiration (see Fig. 1). *Error bars* represent the standard deviation of 3–6 measurements. For clarity, *errors bars* are shown only for ECAR maxima but are in the same order of magnitude for ECAR after 40 min. The *solid line* represents the best fit of Equation 3 to the ECAR data with a dissociation constant for CPT-cAMP, $K_{d,app} = 8.5\ \mu M$ and an $ECAR_{max} = 209\%$. CHO-K1 cells start to respond only at concentrations higher than 50 μM resulting in a maximum ECAR of 130% at 400 μM CPT-cAMP. *B*, ECAR was transformed to the rate of ATP synthesis/hydrolysis taking into account the OCR data of Fig. 1*B*.

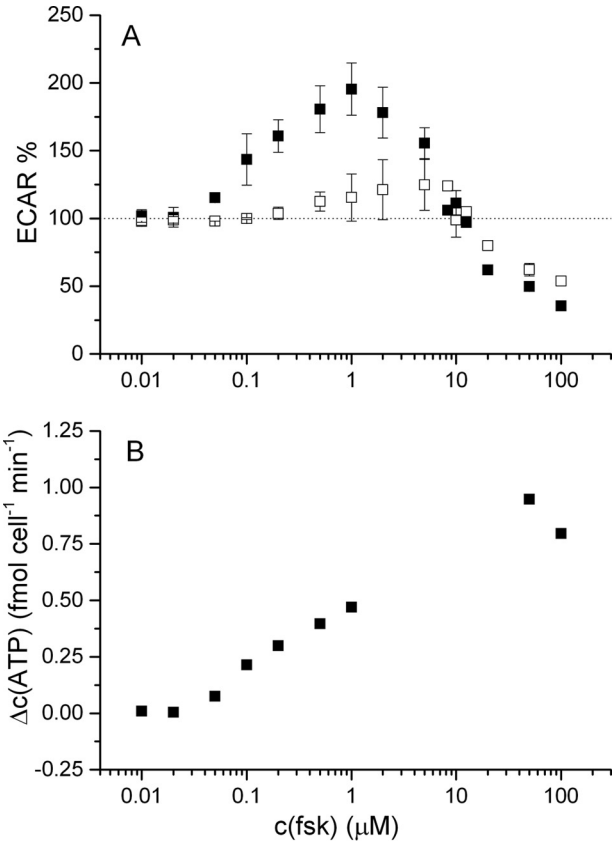

FIGURE 3. ***A* and *B*. ECAR of CHO-K1 and CHO-CFTR cells as a function of forskolin concentration.** ECAR of CHO-K1 (□) and CHO-CFTR (■) cells measured in a Molecular Dynamics Cytosensor at 37 °C for 30 s every 2 min. *A*, last four points of measurements (8 min) during perfusion with forskolin were averaged, normalized to the basal value before stimulation, and plotted against forskolin concentration. *Error bars* represent the standard deviation of 2–4 experiments. ECAR response of CHO-CFTR cells showed an increase at lower and a decrease at higher concentrations with a maximum of 195 ± 19% of basal ECAR at 1 μM forskolin. CHO-K1 cells only responded at concentrations $C_{fsk} > 10\ \mu M$ with a minimal ECAR of 35% at $C_{fsk} = 100\ \mu M$. The *dotted line* shows the basal ECAR to guide the eye. *B*, rate of ATP synthesis/hydrolysis was roughly estimated taking into account the OCR data of Fig. 1*D*.

OCR measurements (Fig. 1*D*). Data in the intermediate concentration range could not be determined accurately and were omitted.

Apparent CFTR-related Catalytic Rate Constant—Upon stimulation of CHO-CFTR cells with CPT-cAMP ($C_{CPT} = 50\ \mu M$), the total CFTR-related basal ATP hydrolysis rate ($v_{bas,H} \approx$

TABLE 2
Inhibition of CFTR Phosphorylation by PKA

Cells were incubated with the PKA inhibitors H-89 and myristoylated PKI(14–22) fragment for 40 or 30 min before stimulation with CPT-cAMP (100 μM) or forskolin (1 μM), and forskolin (50 μM).

Inhibitor	CPT-cAMP (100 μM)	Forskolin (1 μM)	Forskolin (50 μM)
	%	%	%
No inhibitor	180	195	64
PKI (10 μM)	145	143	ND[a]
PKI (20 μM)	115	ND[a]	ND[a]
H89 (20 μM)	110	111	68

[a] ND, not determined.

0.49 fmol cell^{-1} min^{-1}) (Fig. 2, *A* and *B*) increased by $\Delta v_{max} \approx$ 0.48 fmol cell^{-1} min^{-1} (corresponding to 4.82·10^6 ATP cell^{-1} s^{-1}). The number of electrophysiologically active CFTR channels per CHO-CFTR cell was estimated previously by dividing the whole cell current by the single channel amplitude as $E_0 = (3.4447 \pm 0.4171)10^4$.[4] The corresponding CFTR-related apparent ATP turnover number or apparent catalytic rate constant was estimated as shown in Equation 5,

$$k_{cat,\,app} = \frac{\Delta v_{max}}{E_0} = 140 s^{-1} \qquad \text{(Eq. 5)}$$

Notably, the apparent catalytic rate constant obtained in the presence of CPT-cAMP consists of the phospho group transferase activity of PKA and the ATPase activity of CFTR.

PKA Activity Is the Major Contribution and CFTR-ATPase Activity Is the Minor Contribution—To assess the relative contribution of the PKA activity to the total CFTR-related ATP hydrolysis rate, we inhibited the latter with two well known protein kinase inhibitors, the myristoylated PKA inhibitor peptide PKI(14–22) (K_i = 36 nM) and the PKA inhibitor H-89 (K_i = 135 nM). Both were applied at a concentration (C_i = 20 μM) previously proven to completely inhibit PKA activity in live cells (51–53). Cells were incubated with the inhibitors for 30–40 min before stimulation with CPT-cAMP or forskolin. Both inhibitors influenced the ECAR and thus the cell metabolism. PKI(14–22) transiently enhanced the ECAR to about 190%, most likely due to its detergent-like nature; however, the signal returned to basal values during the incubation period. H-89 enhanced the ECAR of all cell lines to about 180% and stabilized at a high level (data not shown). In the case of H-89, observations were therefore normalized to this altered basal activity. Both inhibitors reduced the stimulation with either CPT-cAMP or forskolin to low values of ~110% as summarized in Table 2. The major ATP hydrolysis rate (≥90%) could thus be attributed to phospho group transferase activity of PKA. The strong down-regulation of the ECAR at high forskolin concentrations (C_{fsk} >10 μM) was not influenced by the PKA inhibitors.

Although we could not fully exclude a low prevailing PKA activity, we assumed that the minor (≤10%) remaining contribution to the total CFTR-related ATP hydrolysis rate was due to ATP hydrolysis of partially phosphorylated CFTR. The catalytic rate constant of CFTR-ATPase was estimated as $k_{cat,\,CFTR} \leq 14\ s^{-1}$. This is in the order of the catalytic rate constant of P-glycoprotein (36, 54, 55) and is also in broad agreement with a previous estimate of the catalytic rate constant of fully phosphorylated CFTR, $k_{cat,\,CFTR} = 1–2\ s^{-1}$ (16).

[4] Dr. J. Reinhardt (Novartis, Switzerland), personal communication.

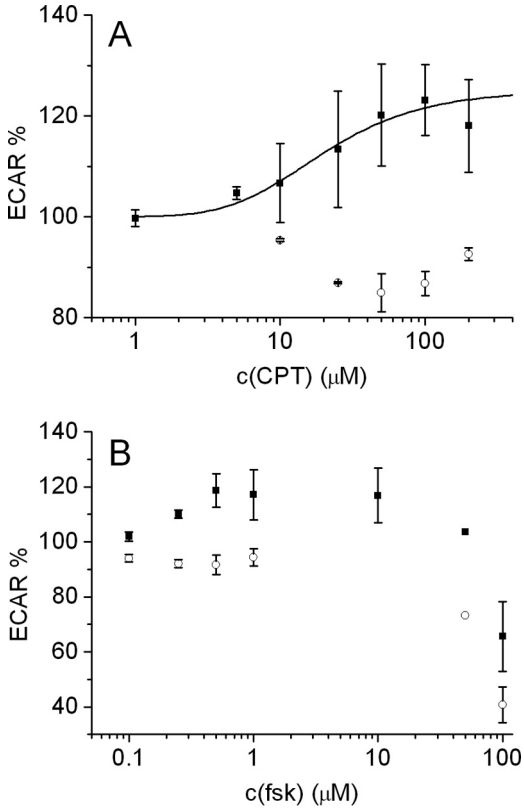

FIGURE 4. ***A* and *B*. ECAR of BHK cells overexpressing CFTR variants as a function of CPT-cAMP and forskolin concentration.** ECAR of BHK-CFTR (■) and BHK-E1371S (○) cells measured in a Molecular Dynamics Cytosensor at 37 °C is shown. *Error bars* represent the standard deviation of 2–4 experiments. *A*, for BHK-CFTR cells stimulation with CPT-cAMP resulted in a maximal ECAR of 123 ± 7% at C_{CPT} = 100 μM; in BHK-E1371S cells the ECAR is slightly reduced to a minimum of 84 ± 4% at C_{CPT} = 50 μM relative to basal values. The *solid line* represents a fit of Equation 3 to data with a dissociation constant for CPT-cAMP, $K_{d,\,app}$ = 3.7 μM and an $ECAR_{max}$ = 125%. *B*, upon titration with forskolin, a maximal ECAR of 117 ± 4% is stably reached for concentrations 0.5 < C_{fsk} ≤ 10 μM in BHK-CFTR cells. BHK-E1371S cells show a reduction down to 91 ± 3% in this concentration range. At concentrations C_{fsk} ≥10 μM, a decrease in ECAR of both cell lines was observed.

CFTR Phosphorylation by PKA—Because PKA activity was responsible for almost the total ECAR or ATP hydrolysis rate in the presence of CPT-cAMP, the ECAR *versus* CPT-cAMP concentration curves obtained with CHO-CFTR and BHK-CFTR cells (Figs. 2, *A* and *B*, and 4*A*) could be well fitted with Equation 3 (44) describing cAMP dissociation from PKA (*i.e.* PKA activation). The resulting apparent dissociation constants, $K_{d,\,app}$, of CPT-cAMP from PKA in both cell lines (for data see Table 1) were in good agreement with previous data, obtained with purified PKA in aqueous solution (56). The good agreement between the behavior of purified and cellular PKA further supports the assumption that the major contribution to CFTR-related ATP hydrolysis was due to PKA activity.

The concentration of half-maximum channel activation by CPT-cAMP was determined as $K_{0.5}$ ≈40 μM at 20 and 40 min. With decreasing incubation times, the parameter, $K_{0.5}$, increased and reached a value of $K_{0.5}$ ~83 μM at 4 min (Table 1), which is in good agreement with a value obtained by patch clamp measurements (9).

CFTR Phosphorylation Occurs in the Post-hydrolysis Transition State—To test whether CFTR-ATPase activity was required for phosphorylation, we used the ATPase-deficient CFTR mutant CFTR-E1371S. It was demonstrated to express well in CHO cells (1), and to exhibit prolonged open times (17). The present experiments were performed with BHK cells under the conditions described above for CHO cells, except that DMEM (without bicarbonate) was used as flow medium instead of MEMα to preserve the conditions used for cell culture. The response of BHK-CFTR cells to stimulation with CPT-cAMP was qualitatively similar to that of CHO-CFTR cells; however, the maximum ECAR was lower (123 ± 7% at C_{CPT} = 100 μM) (Fig. 4*A*). The response to forskolin (Fig. 4*B*) was also similar to that in CHO cells, but the ECAR was again lower and reached a maximum stimulation of 117 ± 4% around C_{fsk} = 1 μM. At higher forskolin concentrations, the ECAR started to decrease as shown above in CHO cells (Fig. 3*A*).

Importantly, BHK-E1371S cells showed no ECAR increase upon addition of phosphorylation agents (Fig. 4). Hence, BHK-E1371S with the hydrolysis-deficient NBD2 was not only unable to hydrolyze ATP, as expected, but moreover could not be phosphorylated. As phosphorylation of BHK-E1371S did not occur, we concluded that ATPase activity is required for phosphorylation and that phosphorylation most likely occurs in the post-hydrolysis transition state. The slight but distinct ECAR decrease (or alkalinization) to 84 ± 4% at C_{CPT} = 50 μM in Fig. 4*A* was most likely due to direct efflux of bicarbonate ions by CFTR-E1371S and possibly also by chloride/bicarbonate exchange proteins regulated indirectly (57, 58).

CFTR-ATPase Activity Is Enhanced by Anion Channel Inhibitors—Next, we investigated how the CFTR-ATPase reacts to chloride channel inhibitors, known to specifically interact with CFTR, including glibenclamide (Fig. 5) glipizide (Fig. 6), and CFTRinh-172 (Fig. 7). For this purpose, we phosphorylated CHO-K1 control cells and CHO-CFTR cells with different CPT-cAMP concentrations (C_{CPT} = 5–100 μM) as described above, whereby phosphorylation was kept constant throughout the subsequent titration experiment. Cells were incubated for 20 min with the particular drugs at each concentration. The interval length and conditions were chosen to ensure that a stable ECAR was reached and the cell metabolism remained glycolytic. After each stimulation period, cells were flushed with medium containing only CPT-cAMP until the ECAR returned to basal values, showing that ECAR changes were reversible at all conditions.

In CHO-K1 cells, anion channel inhibitors induced only negligibly small effects (<120%) except CFTRinh-172, which reached ECAR values of ~138% at C_{CPT} = 50 μM. In CHO-CFTR cells, all there anion channel inhibitors induced bell-shaped CFTR-ATPase activity curves with ECAR maxima up to ~210% (Figs. 5–7). Titration curves could be well fitted with Equation 4 that assumes ATPase activation at low and inhibition at high allocrite concentrations as shown previously for P-glycoprotein in inside-out lipid vesicles (36, 45, 59) and in cells (36, 38). Kinetic analysis (Equation 4) of the titration curves in the presence of different concentrations of CPT-cAMP (Figs. 5–7) yielded the concentration of half-maximum

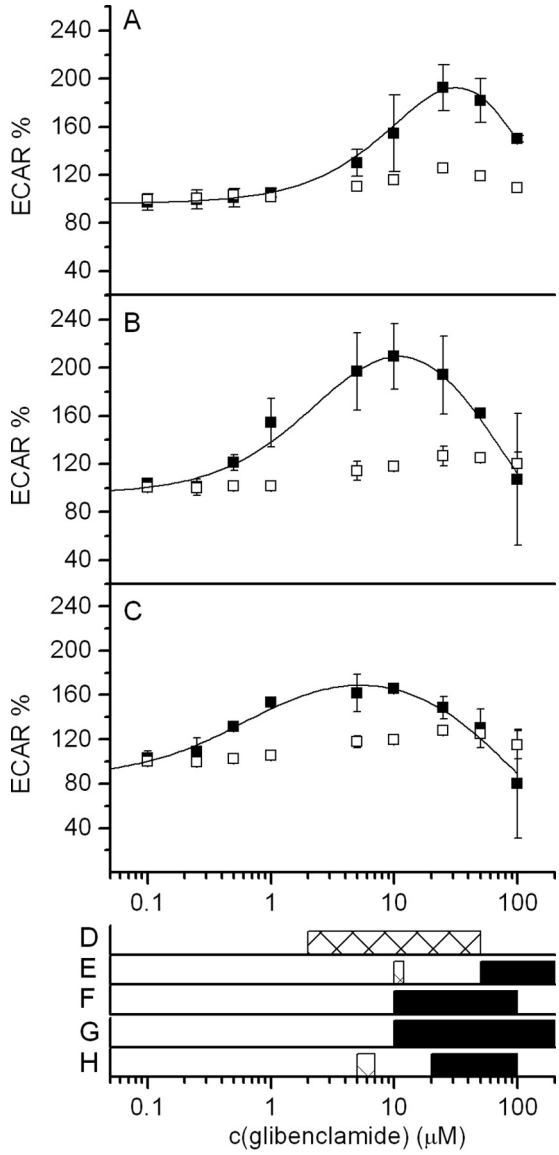

FIGURE 5. ***A–H.* Effect of glibenclamide on ECAR and iodide efflux in comparison with published data on channel function.** *A–C,* ECAR as a function of glibenclamide concentration in CHO-K1 (□) and CHO-CFTR (■) cells after stimulation with CPT-cAMP concentrations C_{CPT} = 5 μM (*A*), C_{CPT} = 25 μM (*B*), or C_{CPT} = 50 μM (*C*). The *solid lines* are fits of Equation 4 to the data. *D,* concentration range where no enhancement (*cross-hatched bars*) of iodide efflux was observed after stimulation with C_{CPT} = 25 μM. It has to be noted that an unspecific increase of iodide efflux in control cells and transfected cells was observed for concentrations C_{glib} ≥10 μM. *E,* glibenclamide concentrations causing no effect (*cross-hatched*) or inhibition (*filled bars*) of short-circuit current stimulated by 100 μM CPT-cAMP in *CFTR*-expressing FRT cells (89). *F,* inhibitory concentrations of glibenclamide detected in analysis of single-channel patch clamp experiments in stably transfected C127 cells in the presence of PKA (90). *G* and *H,* concentration range reported to cause channel block by glibenclamide in excised patches from *Xenopus* oocytes in the presence of 50 units/ml PKA (91). Data obtained from biological triplicates are shown with standard deviations.

CFTR-ATPase activation, K_1, and inhibition, K_2, as well as maximum, V_1, and minimum activity, V_2, summarized in Table 3.

CFTR-ATPase Activity Is Reduced by Anion Channel Potentiators—Analogous titrations of CHO-K1 and CHO-CFTR cells, respectively, were performed with the potentiators genistein (Fig. 8*A*) and capsaicin (Fig. 8*B*). In contrast to inhibitors, potentiators showed no ECAR increase. Higher concen-

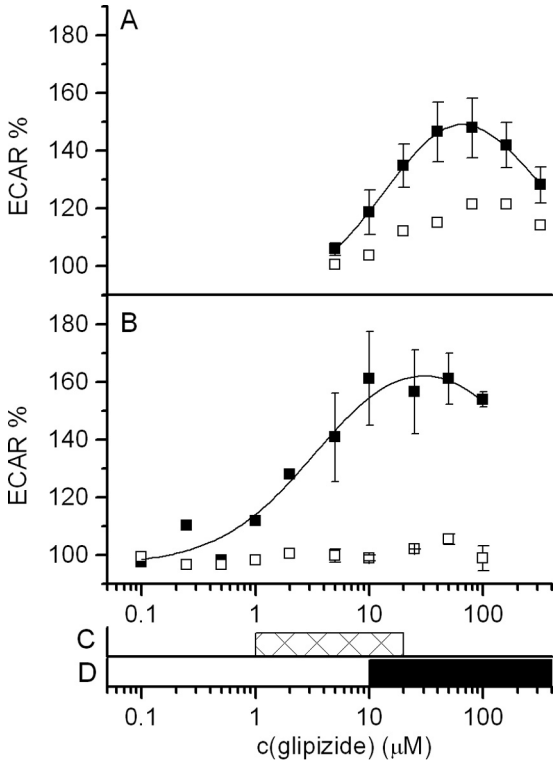

FIGURE 6. ***A* and *B*. Effect of glipizide on ECAR and iodide efflux in comparison with published results on channel function.** *A* and *B*, ECAR as a function of glipizide concentration in CHO-K1 (□) and CHO-CFTR (■) cells after stimulation with C_{CPT} = 25 μM (*A*) or C_{CPT} = 50 μM (*B*). The *solid lines* are fits of Equation 4 to the data. *C*, concentration range where no enhancements on iodide efflux after stimulation with C_{CPT} = 25 μM were observed. *D*, concentration range reported to cause channel block by glipizide in excised patches from *Xenopus* oocytes in the presence of PKA (91). Data obtained from biological duplicates are shown with standard deviations.

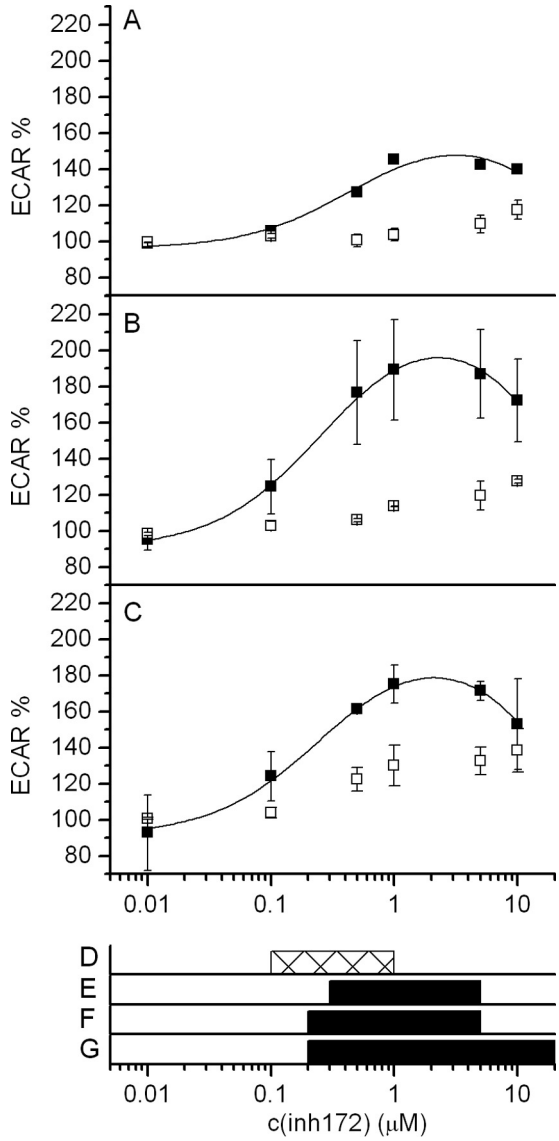

FIGURE 7. ***A–C*. Effects of CFTRinh-172 on ECAR and iodide efflux in comparison with published results on channel function.** *A–C*, ECAR as a function of CFTRinh-172 concentration in CHO K1 (□) and CHO-CFTR (■) cells after stimulation with C_{CPT} = 5 μM (*A*), C_{CPT} = 25 μM (*B*), and C_{CPT} = 50 μM (*C*). The *solid lines* are fits of Equation 4 to the data. *D*, concentration range where no enhancement of channel function was observed in iodide efflux experiments after stimulation with C_{CPT} = 25 μM. *E*, inhibition of channel function described in literature for iodide influx after stimulation with an CFTR activating mixture containing 5 μM forskolin, 100 μM Isobutylmethylxanthine, and 25 μM apigenin (89). *F*, concentration range reported to cause inhibition of CFTR-dependent short-circuit current after stimulation with 100 μM CPT-cAMP (89). *G*, concentration range described to block CFTR in excised patches from transfected mouse embryo fibroblasts (92). Data obtained from biological duplicates are shown with standard deviations.

trations even reduced the ECAR of CHO-K1 and CHO-CFTR cells down to a minimum of ~55 and 35%, respectively, in the case of genistein (Fig. 8*A*) and 65 and 50%, respectively, in the case of capsaicin (Fig. 9*A*). The ECAR decrease at high potentiator concentrations was fully reversible under all conditions in both cell lines.

Anion Channel Potentiators Induce Cellular Respiration—At concentrations relevant for anion channel activation, potentiators such as genistein (Fig. 8) and capsaicin (Fig. 9) significantly reduced ECAR in both CFTR overexpressing (CHO-CFTR) and control (CHO-K1) cells. As for forskolin (47–49), inhibition of glucose import has been observed for several flavonoids, including genistein, *e.g.* in U937 cells (60) and CHO cells (61). To our knowledge, the influence of capsaicin on glucose metabolism has not yet been described. Both potentiators thus seemed to reduce glucose uptake, which leads to a reduction in glycolysis and to an increase in respiration as observed for forskolin (Fig. 1*D*).

CPT-cAMP and Forskolin Not Only Act as Phosphorylation Agents but also as CFTR Modulators—The CFTR-ATPase activity curves were measured at different CPT-cAMP concentrations (Figs. 5–7). With increasing concentrations of CPT-cAMP, the apparent concentration of half-maximum CFTR-ATPase activation, K_1, decreased. The shift to lower values was particularly evident for the more hydrophilic glibenclamide and glipizide (Fig. 7 and Table 3), and it was less pronounced for the more hydrophobic CFTRinh-172. The maximum ATPase activity, V_1, of CFTR, induced by the chloride channel inhibitors (*i.e.* ATPase activators) increased at very low CPT-cAMP concentrations and decreased at higher concentrations (C_{CPT} ≥25 μM). Analogous shifts of kinetic constants of CFTR with the CPT-cAMP concentration were observed previously for the potentiator genistein (62).

The phenomenon described above is typical for ABC transporters such as P-glycoprotein, which are able to simultaneously accommodate different molecules in their binding

TABLE 3

Kinetic constants of the CFTR-ATPase derived from microphysiometry experiments with CHO-CFTR cells in MEMα at pH 7.4 and *T* = 37 °C

The concentration of half-maximum activation (inhibition) K_1 (K_2) and the rate of activation (inhibition) V_1 (V_2) were obtained by fitting Equation 1 to the data.

Compound	C_{CPT}	K_1	K_2	V_1	V_2	$ECAR_{max}$
	μM	μM	μM	%	%	%
Glibenclamide	5	25.0	105.1	315	0	192 ± 19
Glibenclamide	10	9.9	67.3	332	0	214 ± 32
Glibenclamide	25	3.0	68.8	275	0	210 ± 27
Glibenclamide	50	1.0	85.3	192	0	165 ± 16
Glibenclamide	100	1.5	63.4	207	0	166 ± 16
Glipizide	25	56.4	80	231	100	148 ± 10
Glipizide	50	6.25	80	198	100	161 ± 16
CFTRinh-172	5	1.0	2.4	190	130	145
CFTRinh-172	25	0.5	3.8	250	150	189 ± 27
CFTRinh-172	50	0.4	12.7	210	80	175 ± 10

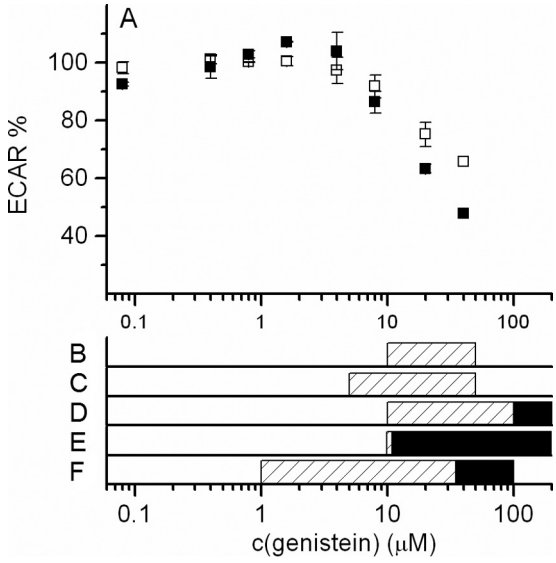

FIGURE 8. ***A–F*. Effects of genistein on ECAR and iodide efflux in comparison with published results on channel function.** *A,* ECAR as a function of genistein concentration in CHO K1 (□) and CHO-CFTR (■) cells after stimulation with C_{CPT} = 50 μM. *B,* concentration range where potentiation (*hatched*) or inhibition (*filled bars*) of channel function was observed in iodide efflux experiments after stimulation with C_{CPT} = 25 μM. *C–F,* effects on channel function described in literature for iodide influx in FRT cells after stimulation with 0.1 μM forskolin (*C*) (93), short-circuit current measurements in the presence of 5 μM (*D*), or 100 μM CPT-cAMP (*E*) (62) or patch clamp measurements in excised patches after stimulation with 0.05 μM forskolin (*F*) (94). *Symbols* have the same meaning as in *B*. Data obtained from biological duplicates are shown with standard deviations.

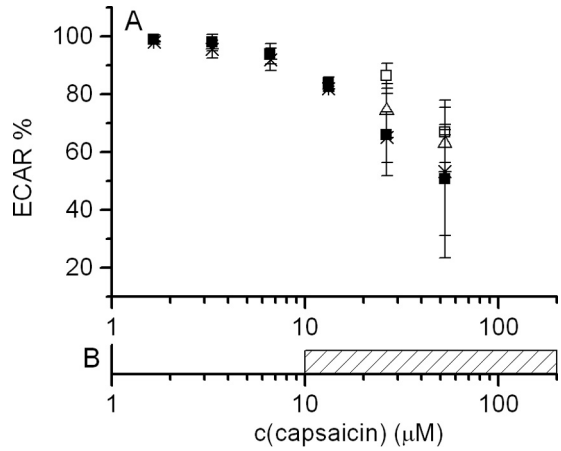

FIGURE 9. ***A* and *B*. Effects of capsaicin on ECAR in comparison with published results on channel function.** *A,* ECAR as a function of capsaicin concentration in CHO K1 (□) in the presence of 50 μM CPT-cAMP and CHO-CFTR cells in the presence of C_{CPT} = 50 μM (■), C_{CPT} = 25 μM (Δ), or C_{CPT} = 5 μM (*). *B,* concentration range reported to cause potentiation by capsaicin whole cell patch clamp experiments in the presence of 10 μM forskolin (95). Data obtained from biological duplicates are shown with standard deviations. Titration curves are fitted with Equation 4.

regions (63–65). The enhanced CFTR-ATPase activity in the presence of very low concentrations of CPT-cAMP and the reduced CFTR-ATPase activity in the presence of higher concentrations of CPT-cAMP thus likely arise from a direct combined modulatory interaction of CPT-cAMP and *e.g.* glibenclamide or glipizide with CFTR. Evidence for binding of cAMP to CFTR has been provided previously (66). Moreover, it is known that ABCC4, which is the ABC transporter most closely related to CFTR, is a cAMP and cGMP exporter (67, 68). CPT-cAMP as well as forskolin may thus not only act as phosphorylation agents but also as modulators of the CFTR-ATPase.

Iodide Efflux at Different Concentrations of Phosphorylation Agents—To be able to directly compare ATPase activity and anion channel activity of CFTR, we used the same cell lines (CHO-CFTR and CHO-K1 cells) for both types of experiments. Moreover, we tested whether cells responded equally in Cytosensor experiments if MEMα was replaced by iodide efflux buffer (2 mM HEPES *versus* 20 mM HEPES). As the basal ECARs were similar under the two conditions, we concluded that a direct comparison of ATP hydrolysis and iodide efflux was warranted. Fig. 10, *A* and *B,* shows the iodide flux at different concentrations of CPT-cAMP and forskolin, respectively, measured as a function of time. At low concentrations, maximum iodide efflux was reached after a 3–4-min incubation time; at high concentrations (C_{fsk} = 50–100 μM) maximum efflux shifted to shorter incubation times of maximally 1 min (data not included). Iodide efflux as a function of time is given in Fig. 10.

ATP-dependent and ATP-independent Increase in Iodide Efflux in the Presence of Phosphorylation Agents—Maximum iodide efflux increased with the concentration of CPT-cAMP (Fig. 11*A*) and reached a first plateau (V_I ≈18.4 fmol cell^{-1} min^{-1}) in the concentration range C_{CPT} = 300–400 μM. Analysis of the ECAR *versus* CPT-cAMP concentration curves (Figs. 2*A* and 4*A*) (see Equation 3) suggests that phosphorylation is completed at C_{CPT} ~400 μM. A further concentration increase to C_{CPT} = 600 μM lead to a further distinct increase in iodide

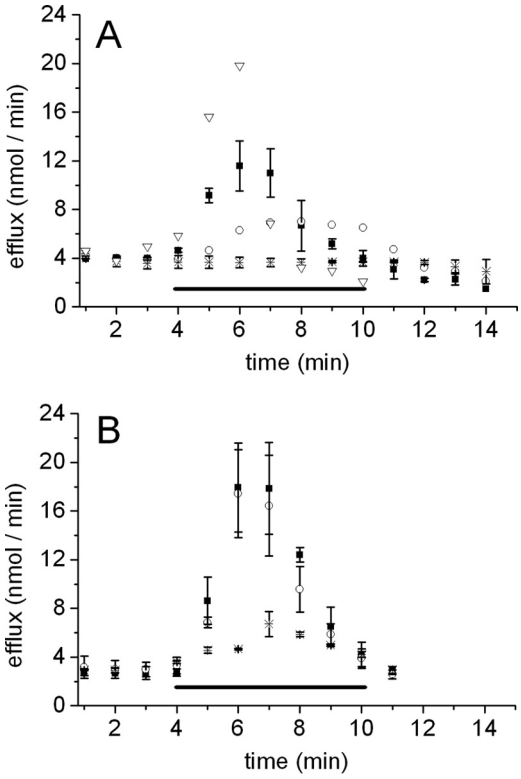

FIGURE 10. ***A* and *B*. Effects of CPT-cAMP and forskolin on iodide efflux of CHO-CFTR cells.** CHO-CFTR cells were loaded with sodium iodide, and the recorded efflux rates were plotted against time. *Horizontal bars* indicate stimulation with 50 μM (*), 100 μM (○), 200 μM (■), and 400 μM (▽) CPT-cAMP (*A*) or with 0.5 μM (*), 5 μM (○) and 10 μM (■) forskolin (*B*).

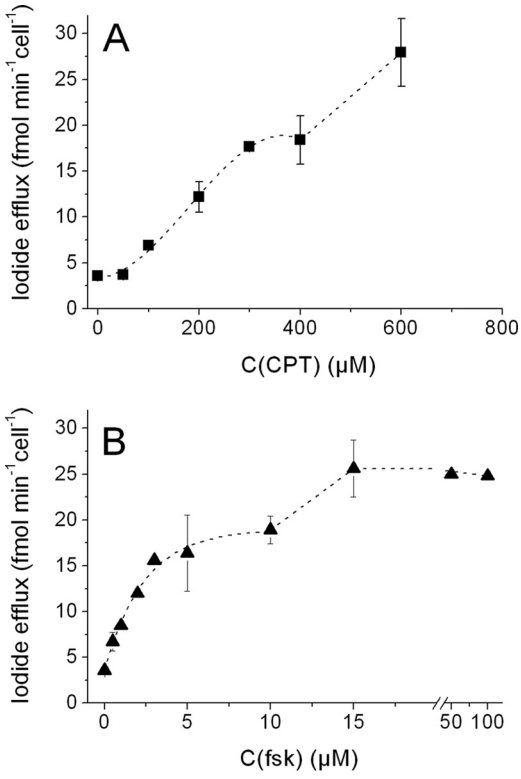

FIGURE 11. ***A* and *B*. Maximum iodide efflux per CHO-CFTR cell as a function of the concentration of phosphorylation agents.** *A,* stimulation with CPT-cAMP (■). *B,* stimulation with forskolin (▲). *Error bars* represent the standard deviation of three experiments. *Dotted lines* were added to guide the eye.

efflux (V_I = 27.9 fmol cell^{-1} min^{-1}). The highest CPT-cAMP concentration measured (C_{CPT} = 1 mM) yielded similar although a slightly lower iodide efflux value, suggesting a second plateau. As the experiment at C_{CPT} = 1 mM was not fully reversible, the value was not included in Fig. 11*A*.

Fig. 11*B* shows an analogous plot for forskolin. The iodide efflux increased with forskolin concentration up to a first plateau (V_I ≈18.9 fmol cell^{-1} min^{-1}) in the concentration range C_{fsk} = 3–10 μM. A concentration of C_{fsk} = 10 μM is generally used (9) to obtain full CFTR phosphorylation. At higher concentrations, again a distinct increase in iodide efflux was observed which lead to a second plateau (V_I ≈25.6 fmol cell^{-1} min^{-1}).

It is interesting to note that iodide efflux increased with the concentration of both phosphorylation agents, first in an ATP-dependent manner up to similar iodide efflux values of ~18 fmol min^{-1} cell^{-1} (first plateau in Fig. 11, *A* and *B*) and second by an ATP-independent manner again up to comparable values (second plateau in Fig. 11). Whereas the first plateau is reached at full phosphorylation of CFTR, the second ATP-independent increase in iodide efflux (see also Fig. 12) can be explained by the modulatory (ATPase inhibitory) effect of phosphorylation agents. The potentially small decrease in iodide efflux at the highest concentrations of phosphorylation agents (C_{CPT} = 1 mM see text and C_{fsk} = 100 μM, see Fig. 11*B*) was rather due to a general metabolic effect than to specific inhibitory phosphorylation sites in CFTR (69).

Iodide Efflux at Different Concentrations of Chloride Channel Inhibitors and Potentiators—Iodide efflux experiments in the presence of chloride channel inhibitors and activators were again performed under conditions closely resembling those in microphysiometry, *i.e.* cells were pre-incubated with CPT-cAMP and were then titrated with the compound of interest. Because higher CPT-cAMP concentrations (C_{CPT} ≥50 μM) strongly enhanced iodide efflux, and lead to a complete iodide efflux from cells within 3 min or less, efflux experiments with chloride channel inhibitors and potentiators were performed with lower CPT-cAMP concentrations. In the presence of CPT-cAMP (C_{CPT} = 25 μM), glibenclamide (C_{glib} = 2–50 μM) (Fig. 5*D*), glipizide (C_{glipz} = 1–20 μM) (Fig. 6*C*), and CFTRinh-172 (C_{inh172} = 0.1–1 μM) (Fig. 7*D*) did not potentiate CFTR-dependent iodide efflux in CHO-CFTR cells. Conversely, genistein (C_{gen} ≥10 μM) distinctly increased iodide efflux under the same conditions (Fig. 8*C*).

As seen from literature data included in the legends to Figs. 5–7, chloride channel inhibitors reduce anion channel activity already in the lower concentration range where ATPase activity increased and reached a maximum. Inhibition persisted at higher concentrations, where ATPase activity decreased again. In the low concentration range where ATPase activity was high, occlusion of the channel is most likely the result of a dynamic process (see "Discussion"). In the high concentration range, occlusion can be explained in terms of the two-site binding model (Equation 4) and most likely results from "static" channel occlusion by inhibitors as described previously (70). As many

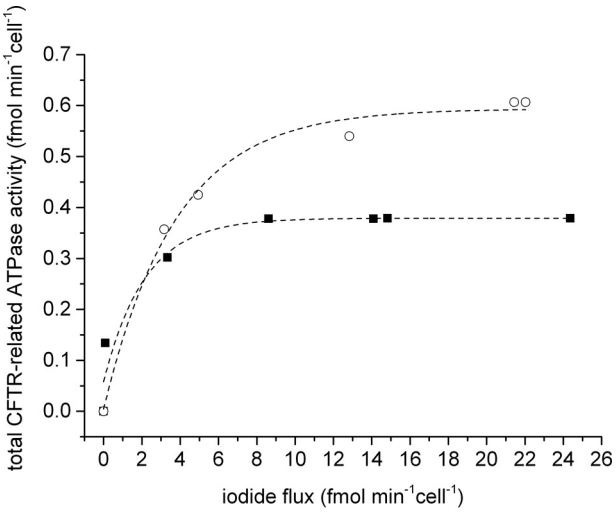

FIGURE 12. **Total CFTR-related ATP hydrolysis rate *versus* maximum iodide efflux.** The total CFTR-related ATP synthesis/hydrolysis rate was derived from ECAR and OCR measurements at superfusion with phosphorylation agents for 6 min to approximate the time frame of iodide efflux measurements more closely. Iodide efflux increased with the total CFTR-related ATP hydrolysis rate up to a certain value in the presence of both CPT-cAMP (■) and forskolin (○). At high concentrations of both phosphorylation agents, the iodide efflux increased in an ATP-independent manner. The amount of ATP required for a given iodide efflux was significantly higher upon phosphorylation with forskolin than upon phosphorylation with CPT-cAMP. Because it can be assumed that PKA and CFTR require the same amount of ATP under both conditions, the surplus in ATP hydrolysis in the presence of forskolin can be attributed to the synthesis of cAMP from ATP catalyzed by adenylate cyclase. *Dotted lines* were added to guide the eye.

CFTR chloride channel inhibitors are anionic amphiphiles, inhibition may be enhanced by repulsive electrostatic interactions.

Conversely, chloride channel potentiators barely enhanced the ATPase activity of CFTR at low concentrations, in agreement with previous investigations (71), and even reduced it at higher concentrations. At the highest concentrations the potentiators also inhibited chloride flux (62) by channel occlusion, most likely again due to more than one molecule bound to the TMDs.

Contribution of Adenylate Cyclase Activity—Whereas CPT-cAMP directly interacts with PKA, forskolin stimulates cAMP synthesis from ATP by activating adenylate cyclase. Because adenylate cyclase activity (72) and phospho group transferase activity of PKA (73) both work in the time frame of minutes, experimental differentiation between the two processes was not possible. To solve this problem, we compared the ATP consumed to induce a given iodide efflux with either CPT-cAMP or forskolin. As seen in Fig. 12, the ATP hydrolysis rates required for a given iodide flux were identical at low concentrations of phosphorylation agents. However, at higher forskolin concentrations (C_{fsk} >1 μM), the ATP hydrolysis rate significantly increased and was clearly higher than in the presence of CPT-cAMP. The higher energy cost in the presence of forskolin can be attributed to the activity of adenylate cyclase.

Estimating CFTR-mediated Iodide Efflux from Loaded Cells—The present data allow a crude estimate of the iodide molecules passing through CFTR per ATP hydrolyzed. If we assume that the catalytic rate constant of the CFTR-ATPase in the presence of high concentrations of CPT-cAMP is on the order of 1% of the total CFTR-related ATP hydrolysis rate ($k_{cat,\ CFTR} \sim 1$ ATP s^{-1}) and that, under these conditions, iodide efflux is ≥30 fmol min^{-1} $cell^{-1}$, the number of iodide molecules flowing out of the iodide-loaded cells through CFTR was estimated as $n \geq 10^4\ s^{-1}$. This number is lower than the average number ($n \approx 10^6\ s^{-1}$) estimated by patch clamp experiments (74). Nevertheless, the data show that the number of anions passing through the channel during one catalytic cycle is high.

Discussion

Here, we provide a detailed analysis of the CFTR-ATPase activity and CFTR phosphorylation by PKA in live cells, using the ECAR and OCR as a proxy for the ATP consumption/hydrolysis rate. In the unperturbed cellular environment, the different ATP-consuming processes could be measured with a good signal to noise ratio that allowed unraveling their influence on CFTR channel gating in an unambiguous manner. Taken together, these results lead to a new model for the catalytic cycle of CFTR.

CFTR Phosphorylation, CFTR-ATPase Activity, and Anion Flux—First, we showed that the total CFTR-related ATP hydrolysis rate (or total, apparent catalytic rate constant) in the presence of CPT-cAMP was $k_{cat,\ app} = 140\ s^{-1}$. The major contribution (≥90%) was due to phosphorylation of the approximately 10 serine residues in the R-domain of CFTR. If phosphorylation was stimulated with forskolin, the rate of ATP hydrolysis was even higher, because adenylate cyclase also contributed (Fig. 12).

The catalytic rate constant of the partially phosphorylated CFTR-ATPase was determined as $k_{cat,\ CFTR} \leq 14\ s^{-1}$. Whether ATPase activity increased (16), stayed constant (75), or even decreased with increasing phosphorylation was at first sight difficult to decide, because of the low basal activity of the CFTR-ATPase compared with the activity of PKA. The good fit of Equation 3 to PKA activity in Figs. 2*A* and 4*A* supports a constant CFTR-ATPase activity. However, data summarized in Table 3 show that CPT-cAMP and forskolin act as modulators in combination with other compounds. The modulator-induced CFTR-ATPase activity showed bell-shaped dependence on concentration and decreased at high concentrations.

Second, we showed that the ATPase-incompetent mutation, CFTR-E1371S, cannot be phosphorylated, suggesting that phosphorylation occurs only if the post-hydrolysis transition state can been reached. Although CFTR-ATPase activity was required for phosphorylation, it was not required for anion flux through CFTR-E1371S, most likely because the mutation as such influences the stability of the protein (76) and may open the ion channel constitutively as shown for a related mutation CFTR-E1371Q (77).

Third, we demonstrated that the ATPase activity of phosphorylated CFTR could be greatly enhanced with anion channel inhibitors but not with anion channel potentiators. The latter rather reduced the ATPase activity of CFTR and, as a side effect, induced a shift from glycolysis to cellular respiration.

Iodide efflux increased with the concentration of phosphorylation agents and reached a first plateau at complete phosphorylation (Fig. 11). Interestingly, further addition of phosphorylation agents led to a further increase in anion efflux without

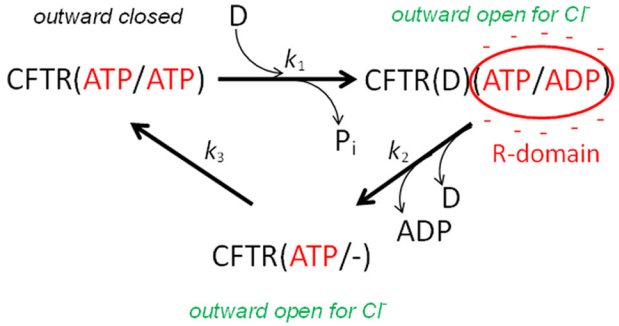

SCHEME 1. **Scheme proposed for the catalytic cycle of CFTR.** CFTR with two molecules of ATP bound (*CFTR(ATP/ATP)*) corresponds to the outward closed conformation (81). In this conformation a drug, *D* (*e.g.* chloride channel potentiator or inhibitor), can enter the cavity from the cytosolic leaflet of the membrane. Upon hydrolysis and release of inorganic phosphate, P_i, the post-hydrolysis transition state of CFTR is reached (*CFTR(D)(ATP/ADP)*). The post-hydrolysis transition state corresponds to the outward open conformation that allows for anion flux through CFTR. In cells the post-hydrolysis transition state is stabilized by the R-domain that adopts a net negative charge upon phosphorylation as indicated by the *red circle*. The high net negative charge in the vicinity of the NBDs may prevent nucleotide exchange by electrostatic repulsion and may delay anion channel closing. CFTR with an empty NBD2 (*CFTR(ATP/−)* is still open but short lived. The rate constant, k_1, includes drug, *D*, binding from the lipid membrane to the TMDs of CFTR and release of inorganic phosphate upon ATP hydrolysis. The rate constant, k_2, includes drug transport or flopping and release, which may be rate-limiting (36, 45) as well as ADP release. The rate constant, k_3, corresponds to ATP binding and concomitant squeeze-out of the drug, *D*, that has not left the transporter cavity before. The apo-conformation was not considered, because the cellular ATP concentration is typically C_{ATP} = 1–10 mM (96, 97), and the concentration of half-maximum activation of CFTR by ATP was determined as $K_{0.5} \approx 50$ μM for CFTR (27).

further stimulation of ATP hydrolysis (Figs. 11 and 12). This further increase in iodide efflux can be explained by the modulatory (ATPase-inhibitory) effect of phosphorylation agents at high concentrations.

New Model for the Catalytic Cycle of CFTR—The strong similarity between ATPase activity curves of CFTR (Figs. 5–7) and ATPase activity curves of P-glycoprotein (59) and Sav1866 (78, 79), a bacterial homolog of P-glycoprotein, suggests that CFTR binds and flips (or rather flops) amphiphilic compounds from the inner to the outer membrane leaflet as the other two transporters. The fact that transport by CFTR has been difficult to observe may be due to fast diffusion of these compounds relative to transport (80). As for P-glycoprotein, CFTR binds and transports a mixed set of allocrites, including, for example, chloride channel inhibitors and the phosphorylation agents CPT-cAMP and forskolin.

Because of these similarities, we tested whether a model for the catalytic cycle of Sav1866, based on molecular dynamics simulations (81), could also be applied to CFTR. The model (Scheme 1) assumes that the transporter remains more or less associated at the NBDs during the whole catalytic cycle (82) and alternates between an outward closed conformation with two identical nucleotides bound (*e.g.* two ATPs or two ADPs) and an outward open conformation, induced by ATP hydrolysis at a single site. This model is in contrast to previous models (see Introduction); however, it is in agreement with the recent investigation of the accessibility of cysteines in CFTR's TMDs by cysteine-reactive probes (34), and it also agrees with the finding that addition of ADP at higher (millimolar) concentrations closes the anion channel of CFTR (83), most likely due to binding of two ADPs.

The fact that hydrolysis was required for phosphorylation to occur pointed to the relevance of the post-hydrolysis transition state. We therefore assumed that the post-hydrolysis transition state corresponds to the open state of the anion channel. The assumption is consistent with previous measurements in inside-out membrane patches showing that efficient stabilization of the open channel was achieved by orthovanadate, known to bind to the post-hydrolysis transition state (84–86). Moreover, it is supported by the observation that non-hydrolyzable ATP analogs do not open (83) CFTR.

Here, we demonstrated that highly ATPase-activating compounds act as chloride channel inhibitors at low and intermediate concentrations (see activating branch of the ATPase activity curve in Figs. 5–7). Inhibition of anion flux occurs most likely, because the dwell time in the outward open conformation (*i.e.* post-hydrolysis transition state) is short compared with the dwell time in the closed conformation. Mechanistically this dynamically closed "state" differs from the occluded state described previously (70). The occluded state is consistent with conditions found at high concentrations of chloride channel inhibitors (*i.e.* decreasing branch of the ATPase activity curve) where most likely more than one molecule is bound to CFTR.

Hence, to obtain significant anion flux, consisting of $\gg 10^4$ s^{-1}, the post-hydrolysis transition state has to be stabilized. We suggest that the role of the highly negatively charged phosphorylated R-domain is to delay nucleotide exchange in the post-hydrolysis transition state and to thereby prolong channel open time. An analogous phosphorylation-dependent slowdown in activity was observed for Rap1 (87).

The open state can also be prolonged by binding of potentiators that reduce the ATPase activity and slow down flopping and drug release (rate constant k_2). As shown for P-glycoprotein, drug release is rate-determining (88).

Upon exchange of ADP at NBD2 for ATP, which leads to a state where two ATPs are bound to the NBDs, the TMDs close at the extracellular side and thereby squeeze out the compounds that have not yet left the cavity toward the extracellular lipid leaflet. At this point the catalytic cycle can restart.

With the present analysis, we demonstrated that measuring the CFTR-related ATP hydrolysis rate in live cells is complementary to electrophysiological measurements of CFTR. Together, the different types of techniques provided a coherent view of the complex interplay between CFTR phosphorylation, CFTR-ATPase activity, and anion channel gating.

Author Contributions—M. Z. and A. S. wrote the manuscript. M. Z., C. E., and A. S. designed the experiments. M. Z., M. H., and C. E. performed the experiments.

Acknowledgments—We are very grateful to Dr. J. R. Riordan (Department of Biochemistry and Biophysics, University of North Carolina School of Medicine) and Dr. J. Reinhardt (Novartis, Switzerland) for providing CHO-CFTR, CHO-ΔF, BHK-CFTR, BHK-ΔF, and BHK-E1371S cells. We thank Dr. Yanyan Xu and Dr. Simon Bernèche for stimulating discussions regarding the catalytic cycle of CFTR.

References

1. Riordan, J. R. (2008) CFTR function and prospects for therapy. *Annu. Rev. Biochem.* **77,** 701–726
2. Qin, L., Zheng, J., Grant, C. E., Jia, Z., Cole, S. P., and Deeley, R. G. (2008) Residues responsible for the asymmetric function of the nucleotide binding domains of multidrug resistance protein 1. *Biochemistry* **47,** 13952–13965
3. Gadsby, D. C., Vergani, P., and Csanády, L. (2006) The ABC protein turned chloride channel whose failure causes cystic fibrosis. *Nature* **440,** 477–483
4. Bozoky, Z., Krzeminski, M., Chong, P. A., and Forman-Kay, J. D. (2013) Structural changes of CFTR R region upon phosphorylation: a plastic platform for intramolecular and intermolecular interactions. *FEBS J.* **280,** 4407–4416
5. Aleksandrov, A. A., and Riordan, J. R. (1998) Regulation of CFTR ion channel gating by MgATP. *FEBS Lett.* **431,** 97–101
6. Cheng, S. H., Rich, D. P., Marshall, J., Gregory, R. J., Welsh, M. J., and Smith, A. E. (1991) Phosphorylation of the R domain by cAMP-dependent protein kinase regulates the CFTR chloride channel. *Cell* **66,** 1027–1036
7. Rosenberg, M. F., O'Ryan, L. P., Hughes, G., Zhao, Z., Aleksandrov, L. A., Riordan, J. R., and Ford, R. C. (2011) The cystic fibrosis transmembrane conductance regulator (CFTR): three-dimensional structure and localization of a channel gate. *J. Biol. Chem.* **286,** 42647–42654
8. Dawson, R. J., and Locher, K. P. (2006) Structure of a bacterial multidrug ABC transporter. *Nature* **443,** 180–185
9. Moran, O., and Zegarra-Moran, O. (2008) On the measurement of the functional properties of the CFTR. *J. Cyst. Fibros.* **7,** 483–494
10. Tabcharani, J. A., Chang, X. B., Riordan, J. R., and Hanrahan, J. W. (1991) Phosphorylation-regulated Cl^- channel in CHO cells stably expressing the cystic fibrosis gene. *Nature* **352,** 628–631
11. Anderson, M. P., Berger, H. A., Rich, D. P., Gregory, R. J., Smith, A. E., and Welsh, M. J. (1991) Nucleoside triphosphates are required to open the CFTR chloride channel. *Cell* **67,** 775–784
12. Gadsby, D. C., and Nairn, A. C. (1999) Regulation of CFTR Cl^- ion channels by phosphorylation and dephosphorylation. *Adv. Second Messenger Phosphoprotein Res.* **33,** 79–106
13. Bear, C. E., Li, C. H., Kartner, N., Bridges, R. J., Jensen, T. J., Ramjeesingh, M., and Riordan, J. R. (1992) Purification and functional reconstitution of the cystic fibrosis transmembrane conductance regulator (CFTR). *Cell* **68,** 809–818
14. Li, C., Ramjeesingh, M., Wang, W., Garami, E., Hewryk, M., Lee, D., Rommens, J. M., Galley, K., and Bear, C. E. (1996) ATPase activity of the cystic fibrosis transmembrane conductance regulator. *J. Biol. Chem.* **271,** 28463–28468
15. Aleksandrov, A. A., Aleksandrov, L., and Riordan, J. R. (2002) Nucleoside triphosphate pentose ring impact on CFTR gating and hydrolysis. *FEBS Lett.* **518,** 183–188
16. Kogan, I., Ramjeesingh, M., and Bear, C. E. (2004) ATPase assay of purified, reconstituted CFTR protein. *J. Cyst. Fibros.* **3,** 133–134
17. Vergani, P., Nairn, A. C., and Gadsby, D. C. (2003) On the mechanism of MgATP-dependent gating of CFTR Cl^- channels. *J. Gen. Physiol.* **121,** 17–36
18. Gadsby, D. C., and Nairn, A. C. (1999) Control of CFTR channel gating by phosphorylation and nucleotide hydrolysis. *Physiol. Rev.* **79,** S77–S107
19. Gregory, R. J., Cheng, S. H., Rich, D. P., Marshall, J., Paul, S., Hehir, K., Ostedgaard, L., Klinger, K. W., Welsh, M. J., and Smith, A. E. (1990) Expression and characterization of the cystic fibrosis transmembrane conductance regulator. *Nature* **347,** 382–386
20. Al-Nakkash, L., and Hwang, T. C. (1999) Activation of wild-type and ΔF508-CFTR by phosphodiesterase inhibitors through cAMP-dependent and -independent mechanisms. *Pflugers Arch.* **437,** 553–561
21. Wang, F., Zeltwanger, S., Hu, S., and Hwang, T. C. (2000) Deletion of phenylalanine 508 causes attenuated phosphorylation-dependent activation of CFTR chloride channels. *J. Physiol.* **524,** 637–648
22. Baldursson, O., Berger, H. A., and Welsh, M. J. (2000) Contribution of R domain phosphoserines to the function of CFTR studied in Fischer rat thyroid epithelia. *Am. J. Physiol. Lung Cell. Mol. Physiol.* **279,** L835–L841
23. Chang, X. B., Tabcharani, J. A., Hou, Y. X., Jensen, T. J., Kartner, N., Alon, N., Hanrahan, J. W., and Riordan, J. R. (1993) Protein kinase A (PKA) still activates CFTR chloride channel after mutagenesis of all 10 PKA consensus phosphorylation sites. *J. Biol. Chem.* **268,** 11304–11311
24. Csanády, L., Chan, K. W., Seto-Young, D., Kopsco, D. C., Nairn, A. C., and Gadsby, D. C. (2000) Severed channels probe regulation of gating of cystic fibrosis transmembrane conductance regulator by its cytoplasmic domains. *J. Gen. Physiol.* **116,** 477–500
25. Winter, M. C., and Welsh, M. J. (1997) Stimulation of CFTR activity by its phosphorylated R domain. *Nature* **389,** 294–296
26. Mathews, C. J., Tabcharani, J. A., Chang, X. B., Jensen, T. J., Riordan, J. R., and Hanrahan, J. W. (1998) Dibasic protein kinase A sites regulate bursting rate and nucleotide sensitivity of the cystic fibrosis transmembrane conductance regulator chloride channel. *J. Physiol.* **508,** 365–377
27. Vergani, P., Lockless, S. W., Nairn, A. C., and Gadsby, D. C. (2005) CFTR channel opening by ATP-driven tight dimerization of its nucleotide-binding domains. *Nature* **433,** 876–880
28. Hwang, T. C., and Sheppard, D. N. (2009) Gating of the CFTR Cl^- channel by ATP-driven nucleotide-binding domain dimerisation. *J. Physiol.* **587,** 2151–2161
29. Csanády, L., Vergani, P., and Gadsby, D. C. (2010) Strict coupling between CFTR's catalytic cycle and gating of its Cl^- ion pore revealed by distributions of open channel burst durations. *Proc. Natl. Acad. Sci. U.S.A.* **107,** 1241–1246
30. Jardetzky, O. (1966) Simple allosteric model for membrane pumps. *Nature* **211,** 969–970
31. Higgins, C. F., and Linton, K. J. (2004) The ATP switch model for ABC transporters. *Nat. Struct. Mol. Biol.* **11,** 918–926
32. Dawson, R. J., and Locher, K. P. (2007) Structure of the multidrug ABC transporter Sav1866 from *Staphylococcus aureus* in complex with AMP-PNP. *FEBS Lett.* **581,** 935–938
33. Aller, S. G., Yu, J., Ward, A., Weng, Y., Chittaboina, S., Zhuo, R., Harrell, P. M., Trinh, Y. T., Zhang, Q., Urbatsch, I. L., and Chang, G. (2009) Structure of P-glycoprotein reveals a molecular basis for poly-specific drug binding. *Science* **323,** 1718–1722
34. Wang, W., and Linsdell, P. (2012) Alternating access to the transmembrane domain of the ATP-binding cassette protein cystic fibrosis transmembrane conductance regulator (ABCC7). *J. Biol. Chem.* **287,** 10156–10165
35. McConnell, H. M., Owicki, J. C., Parce, J. W., Miller, D. L., Baxter, G. T., Wada, H. G., and Pitchford, S. (1992) The cytosensor microphysiometer: biological applications of silicon technology. *Science* **257,** 1906–1912
36. Aänismaa, P., and Seelig, A. (2007) P-glycoprotein kinetics measured in plasma membrane vesicles and living cells. *Biochemistry* **46,** 3394–3404
37. Gatlik-Landwojtowicz, E., Aänismaa, P., and Seelig, A. (2004) The rate of P-glycoprotein activation depends on the metabolic state of the cell. *Biochemistry* **43,** 14840–14851
38. Gatlik-Landwojtowicz, E., Aänismaa, P., and Seelig, A. (2006) Quantification and characterization of P-glycoprotein-substrate interactions. *Biochemistry* **45,** 3020–3032
39. Thedinga, E., Kob, A., Holst, H., Keuer, A., Drechsler, S., Niendorf, R., Baumann, W., Freund, I., Lehmann, M., and Ehret, R. (2007) Online monitoring of cell metabolism for studying pharmacodynamic effects. *Toxicol. Appl. Pharmacol.* **220,** 33–44
40. Hafner, F. (2000) Cytosensor Microphysiometer: technology and recent applications. *Biosens Bioelectron* **15,** 149–158
41. Landwojtowicz, E., Nervi, P., and Seelig, A. (2002) Real-time monitoring of P-glycoprotein activation in living cells. *Biochemistry* **41,** 8050–8057
42. Owicki, J. C., Parce, J. W., Kercso, K. M., Sigal, G. B., Muir, V. C., Venter, J. C., Fraser, C. M., and McConnell, H. M. (1990) Continuous monitoring of receptor-mediated changes in the metabolic rates of living cells. *Proc. Natl. Acad. Sci. U.S.A.* **87,** 4007–4011
43. Chen, E. Y., Bartlett, M. C., Loo, T. W., and Clarke, D. M. (2004) The ΔF508 mutation disrupts packing of the transmembrane segments of the cystic fibrosis transmembrane conductance regulator. *J. Biol. Chem.* **279,** 39620–39627
44. Moran, O. (2010) Model of the cAMP activation of chloride transport by

CFTR channel and the mechanism of potentiators. *J. Theor. Biol.* **262,** 73–79
45. Litman, T., Zeuthen, T., Skovsgaard, T., and Stein, W. D. (1997) Structure-activity relationships of P-glycoprotein interacting drugs: kinetic characterization of their effects on ATPase activity. *Biochim. Biophys. Acta* **1361,** 159–168
46. Lin, S. J., Kaeberlein, M., Andalis, A. A., Sturtz, L. A., Defossez, P. A., Culotta, V. C., Fink, G. R., and Guarente, L. (2002) Calorie restriction extends *Saccharomyces cerevisiae* lifespan by increasing respiration. *Nature* **418,** 344–348
47. van Valen, F., and Keck, E. (1988) Forskolin inhibition of glucose transport in bone cell cultures through a cAMP-independent mechanism. *Bone* **9,** 89–92
48. Geisbuhler, T. P., Sergeant, S., Miramonti, F. L., Kim, H. D., and Rovetto, M. J. (1987) Forskolin inhibition of hexose transport in cardiomyocytes. *Pflugers Arch.* **409,** 158–162
49. Sergeant, S., and Kim, H. D. (1985) Inhibition of 3-*O*-methylglucose transport in human erythrocytes by forskolin. *J. Biol. Chem.* **260,** 14677–14682
50. Guarino, R. D., Dike, L. E., Haq, T. A., Rowley, J. A., Pitner, J. B., and Timmins, M. R. (2004) Method for determining oxygen consumption rates of static cultures from microplate measurements of pericellular dissolved oxygen concentration. *Biotechnol. Bioeng.* **86,** 775–787
51. Laohapitakworn, S., Thongbunchoo, J., Nakkrasae, L. I., Krishnamra, N., and Charoenphandhu, N. (2011) Parathyroid hormone (PTH) rapidly enhances CFTR-mediated HCO secretion in intestinal epithelium-like Caco-2 monolayer: a novel ion regulatory action of PTH. *Am. J. Physiol. Cell Physiol.* **301,** C137–C149
52. Hughes, L. K., Ju, M., and Sheppard, D. N. (2008) Potentiation of cystic fibrosis transmembrane conductance regulator (CFTR) Cl^- currents by the chemical solvent tetrahydrofuran. *Mol. Membr. Biol.* **25,** 528–538
53. Wu, D., and Hu, Z. (2008) Rutaecarpine induces chloride secretion across rat isolated distal colon. *J. Pharmacol. Exp. Ther.* **325,** 256–266
54. Ambudkar, S. V., Cardarelli, C. O., Pashinsky, I., and Stein, W. D. (1997) Relation between the turnover number for vinblastine transport and for vinblastine-stimulated ATP hydrolysis by human P-glycoprotein. *J. Biol. Chem.* **272,** 21160–21166
55. Al-Shawi, M. K., Polar, M. K., Omote, H., and Figler, R. A. (2003) Transition state analysis of the coupling of drug transport to ATP hydrolysis by P-glycoprotein. *J. Biol. Chem.* **278,** 52629–52640
56. Dao, K. K., Teigen, K., Kopperud, R., Hodneland, E., Schwede, F., Christensen, A. E., Martinez, A., and Døskeland, S. O. (2006) Epac1 and cAMP-dependent protein kinase holoenzyme have similar cAMP affinity, but their cAMP domains have distinct structural features and cyclic nucleotide recognition. *J. Biol. Chem.* **281,** 21500–21511
57. Luckie, D. B., Singh, C. N., Wine, J. J., and Wilterding, J. H. (2001) CFTR activation raises extracellular pH of NIH/3T3 mouse fibroblasts and C127 epithelial cells. *J. Membr. Biol.* **179,** 275–284
58. Tang, L., Fatehi, M., and Linsdell, P. (2009) Mechanism of direct bicarbonate transport by the CFTR anion channel. *J. Cyst. Fibros.* **8,** 115–121
59. Egido, E., Müller, R., Li-Blatter, X., Merino, G., and Seelig, A. (2015) Predicting activators and inhibitors of the breast cancer resistance protein (ABCG2) and P-glycoprotein (ABCB1) based on mechanistic considerations. *Mol. Pharm.* **12,** 4026–4037
60. Park, J. B. (1999) Flavonoids are potential inhibitors of glucose uptake in U937 cells. *Biochem. Biophys. Res. Commun.* **260,** 568–574
61. Vera, J. C., Reyes, A. M., Cárcamo, J. G., Velásquez, F. V., Rivas, C. I., Zhang, R. H., Strobel, P., Iribarren, R., Scher, H. I., and Slebe, J. C. (1996) Genistein is a natural inhibitor of hexose and dehydroascorbic acid transport through the glucose transporter, GLUT1. *J. Biol. Chem.* **271,** 8719–8724
62. Moran, O., and Zegarra-Moran, O. (2005) A quantitative description of the activation and inhibition of CFTR by potentiators: Genistein. *FEBS Lett.* **579,** 3979–3983
63. Litman, T., Zeuthen, T., Skovsgaard, T., and Stein, W. D. (1997) Competitive, non-competitive and cooperative interactions between substrates of P-glycoprotein as measured by its ATPase activity. *Biochim. Biophys. Acta* **1361,** 169–176
64. Li-Blatter, X., Nervi, P., and Seelig, A. (2009) Detergents as intrinsic P-glycoprotein substrates and inhibitors. *Biochim. Biophys. Acta* **1788,** 2335–2344
65. Ernst, R., Kueppers, P., Stindt, J., Kuchler, K., and Schmitt, L. (2010) Multidrug efflux pumps: substrate selection in ATP-binding cassette multidrug efflux pumps–first come, first served? *FEBS J.* **277,** 540–549
66. Pereira, M. M., Parker, J., Stratford, F. L., McPherson, M., and Dormer, R. L. (2007) Activation mechanisms for the cystic fibrosis transmembrane conductance regulator protein involve direct binding of cAMP. *Biochem. J.* **405,** 181–189
67. Wielinga, P. R., van der Heijden, I., Reid, G., Beijnen, J. H., Wijnholds, J., and Borst, P. (2003) Characterization of the MRP4- and MRP5-mediated transport of cyclic nucleotides from intact cells. *J. Biol. Chem.* **278,** 17664–17671
68. Klein, I., Sarkadi, B., and Váradi, A. (1999) An inventory of the human ABC proteins. *Biochim. Biophys. Acta* **1461,** 237–262
69. Csanády, L., Seto-Young, D., Chan, K. W., Cenciarelli, C., Angel, B. B., Qin, J., McLachlin, D. T., Krutchinsky, A. N., Chait, B. T., Nairn, A. C., and Gadsby, D. C. (2005) Preferential phosphorylation of R-domain serine 768 dampens activation of CFTR channels by PKA. *J. Gen. Physiol.* **125,** 171–186
70. Linsdell, P. (2014) Cystic fibrosis transmembrane conductance regulator chloride channel blockers: pharmacological, biophysical and physiological relevance. *World J. Biol. Chem.* **5,** 26–39
71. Eckford, P. D., Li, C., Ramjeesingh, M., and Bear, C. E. (2012) Cystic fibrosis transmembrane conductance regulator (CFTR) potentiator VX-770 (ivacaftor) opens the defective channel gate of mutant CFTR in a phosphorylation-dependent but ATP-independent manner. *J. Biol. Chem.* **287,** 36639–36649
72. Salomon, Y., Londos, C., and Rodbell, M. (1974) A highly sensitive adenylate cyclase assay. *Anal. Biochem.* **58,** 541–548
73. Hegedus, T., Aleksandrov, A., Mengos, A., Cui, L., Jensen, T. J., and Riordan, J. R. (2009) Role of individual R domain phosphorylation sites in CFTR regulation by protein kinase A. *Biochim. Biophys. Acta* **1788,** 1341–1349
74. Muallem, D., and Vergani, P. (2009) Review. ATP hydrolysis-driven gating in cystic fibrosis transmembrane conductance regulator. *Philos. Trans. R. Soc. Lond. B Biol. Sci.* **364,** 247–255
75. Ketchum, C. J., Rajendrakumar, G. V., and Maloney, P. C. (2004) Characterization of the adenosinetriphosphatase and transport activities of purified cystic fibrosis transmembrane conductance regulator. *Biochemistry* **43,** 1045–1053
76. Csanády, L., Mihályi, C., Szollosi, A., Töröcsik, B., and Vergani, P. (2013) Conformational changes in the catalytically inactive nucleotide-binding site of CFTR. *J. Gen. Physiol.* **142,** 61–73
77. Zhou, J. J., Li, M. S., Qi, J., and Linsdell, P. (2010) Regulation of conductance by the number of fixed positive charges in the intracellular vestibule of the CFTR chloride channel pore. *J. Gen. Physiol.* **135,** 229–245
78. Velamakanni, S., Yao, Y., Gutmann, D. A., and van Veen, H. W. (2008) Multidrug transport by the ABC transporter Sav1866 from *Staphylococcus aureus*. *Biochemistry* **47,** 9300–9308
79. Beck, A., Aänismaa, P., Li-Blatter, X., Dawson, R., Locher, K., and Seelig, A. (2013) Sav1866 from *Staphylococcus aureus* and P-glycoprotein: similarities and differences in ATPase activity assessed with detergents as allocrites. *Biochemistry* **52,** 3297–3309
80. Seelig, A. (2007) The role of size and charge for blood-brain barrier permeation of drugs and fatty acids. *J. Mol. Neurosci.* **33,** 32–41
81. Xu, Y. (2014) *Molecular Mechanics Investigation of the Transport Mechanisms in the ClC-ec1 H^+/ Cl^- Exchanger and P- glycoprotein/Sav1866 ABC Transporter*. Ph.D. thesis, University of Basel, Basel, Switzerland
82. Szollosi, A., Muallem, D. R., Csanády, L., and Vergani, P. (2011) Mutant cycles at CFTR's non-canonical ATP-binding site support little interface separation during gating. *J. Gen. Physiol.* **137,** 549–562
83. Schultz, B. D., Venglarik, C. J., Bridges, R. J., and Frizzell, R. A. (1995) Regulation of CFTR Cl^- channel gating by ADP and ATP analogues. *J. Gen. Physiol.* **105,** 329–361
84. Baukrowitz, T., Hwang, T. C., Nairn, A. C., and Gadsby, D. C. (1994) Coupling of CFTR Cl^- channel gating to an ATP hydrolysis cycle. *Neuron* **12,** 473–482

85. Gunderson, K. L., and Kopito, R. R. (1994) Effects of pyrophosphate and nucleotide analogs suggest a role for ATP hydrolysis in cystic fibrosis transmembrane regulator channel gating. *J. Biol. Chem.* **269,** 19349–19353
86. Basso, C., Vergani, P., Nairn, A. C., and Gadsby, D. C. (2003) Prolonged nonhydrolytic interaction of nucleotide with CFTR's NH2-terminal nucleotide binding domain and its role in channel gating. *J. Gen. Physiol.* **122,** 333–348
87. Takahashi, M., Dillon, T. J., Liu, C., Kariya, Y., Wang, Z., and Stork, P. J. (2013) Protein kinase A-dependent phosphorylation of Rap1 regulates its membrane localization and cell migration. *J. Biol. Chem.* **288,** 27712–27723
88. Li-Blatter, X., Beck, A., and Seelig, A. (2012) P-glycoprotein-ATPase modulation: the molecular mechanisms. *Biophys. J.* **102,** 1383–1393
89. Ma, T., Thiagarajah, J. R., Yang, H., Sonawane, N. D., Folli, C., Galietta, L. J., and Verkman, A. S. (2002) Thiazolidinone CFTR inhibitor identified by high-throughput screening blocks cholera toxin-induced intestinal fluid secretion. *J. Clin. Invest.* **110,** 1651–1658
90. Sheppard, D. N., and Robinson, K. A. (1997) Mechanism of glibenclamide inhibition of cystic fibrosis transmembrane conductance regulator Cl^- channels expressed in a murine cell line. *J. Physiol.* **503,** 333–346
91. Cui, G., Song, B., Turki, H. W., and McCarty, N. A. (2012) Differential contribution of TM6 and TM12 to the pore of CFTR identified by three sulfonylurea-based blockers. *Pflugers Arch* **463,** 405–418
92. Kopeikin, Z., Sohma, Y., Li, M., and Hwang, T. C. (2010) On the mechanism of CFTR inhibition by a thiazolidinone derivative. *J. Gen. Physiol.* **136,** 659–671
93. Galietta, L. V., Jayaraman, S., and Verkman, A. S. (2001) Cell-based assay for high-throughput quantitative screening of CFTR chloride transport agonists. *Am. J. Physiol. Cell Physiol.* **281,** C1734–C1742
94. Wang, F., Zeltwanger, S., Yang, I. C., Nairn, A. C., and Hwang, T. C. (1998) Actions of genistein on cystic fibrosis transmembrane conductance regulator channel gating. Evidence for two binding sites with opposite effects. *J. Gen. Physiol.* **111,** 477–490
95. Ai, T., Bompadre, S. G., Wang, X., Hu, S., Li, M., and Hwang, T. C. (2004) Capsaicin potentiates wild-type and mutant cystic fibrosis transmembrane conductance regulator chloride-channel currents. *Mol. Pharmacol.* **65,** 1415–1426
96. Ataullakhanov, F. I., and Vitvitsky, V. M. (2002) What determines the intracellular ATP concentration. *Biosci. Rep.* **22,** 501–511
97. Beis, I., and Newsholme, E. A. (1975) The contents of adenine nucleotides, phosphagens and some glycolytic intermediates in resting muscles from vertebrates and invertebrates. *Biochem. J.* **152,** 23–32

ADDITIONS AND CORRECTIONS

THE JOURNAL OF BIOLOGICAL CHEMISTRY VOL. 291, NO. 46, p. 23928, November 11, 2016

VOLUME 291 (2016) PAGES 14483–14498
DOI 10.1074/jbc.A116.721415

How phosphorylation and ATPase activity regulate anion flux through the cystic fibrosis transmembrane conductance regulator (CFTR).

Matthias Zwick, Cinzia Esposito, Manuel Hellstern, and Anna Seelig

A word was misspelled in the title. The correct title is shown above.

Authors are urged to introduce these corrections into any reprints they distribute. Secondary (abstract) services are urged to carry notice of these corrections as prominently as they carried the original abstracts.

How Phosphorylation and ATPase Activity Regulate Anion Flux though the Cystic Fibrosis Transmembrane Conductance Regulator (CFTR)

Matthias Zwick, Cinzia Esposito, Manuel Hellstern and Anna Seelig

J. Biol. Chem. 2016, 291:14483-14498.
doi: 10.1074/jbc.M116.721415 originally published online May 12, 2016
